Space Sci Rev (2012) 173:247–281
DOI 10.1007/s11214-012-9932-y

Shock Acceleration of Ions in the Heliosphere

Martin A. Lee · R.A. Mewaldt · J. Giacalone

Received: 17 April 2012 / Accepted: 22 August 2012 / Published online: 22 September 2012

Abstract Energetic particles constitute an important component of the heliospheric plasma environment. They range from solar energetic particles in the inner heliosphere to the anomalous cosmic rays accelerated at the interface of the heliosphere with the local interstellar medium. Although stochastic acceleration by fluctuating electric fields and processes associated with magnetic reconnection may account for some of the particle populations, the majority are accelerated by the variety of shock waves present in the solar wind. This review focuses on "gradual" solar energetic particle (SEP) events including their energetic storm particle (ESP) phase, which is observed if and when an associated shock wave passes Earth. Gradual SEP events are the intense long-duration events responsible for most space weather disturbances of Earth's magnetosphere and upper atmosphere. The major characteristics of gradual SEP events are first described including their association with shocks and coronal mass ejections (CMEs), their ion composition, and their energy spectra. In the context of acceleration mechanisms in general, the acceleration mechanism responsible for SEP events, diffusive shock acceleration, is then described in some detail including its predictions for a planar stationary shock, shock modification by the energetic particles, and wave excitation by the accelerating ions. Finally, some complexities of shock acceleration are addressed, which affect the predictive ability of the theory. These include the role of temporal and spatial variations, the distinction between the plasma and wave compression ratios at the shock, the injection of thermal plasma at the shock into the process of shock acceleration, and the nonlinear evolution of ion-excited waves in the vicinity of the shock.

Keywords Particle acceleration · Solar energetic particles · Diffusive shock acceleration

M.A. Lee (✉)
Space Science Center, University of New Hampshire, Morse Hall, 8 College Rd., Durham, NH 03824, USA
e-mail: marty.lee@unh.edu

R.A. Mewaldt
California Institute of Technology, 290-17 Cahill Laboratory, Pasadena, CA 91125, USA

J. Giacalone
Department of Planetary Sciences, University of Arizona, 1629 E. University Blvd., Tucson, AZ 85721, USA

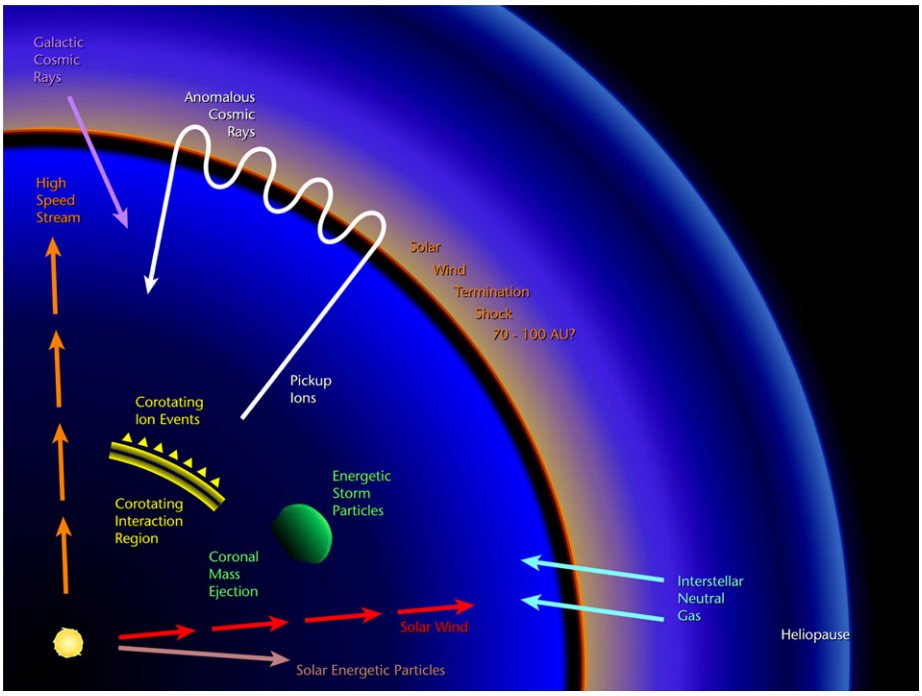

Fig. 1 Schematic diagram of the Sun, solar wind termination shock, and heliopause, with key particle populations including the solar wind, solar energetic particles, energetic storm particles, corotating energetic ion events, anomalous cosmic rays, galactic cosmic rays, and the interstellar neutral gas [Illustration by Eric Christian for the cover of *Acceleration and Transport of Energetic Particles Observed in the Heliosphere* (Mewaldt et al. 2000)]

1 Introduction

Populations of energetic ions and electrons are major constituents of the heliospheric plasma environment. They are ubiquitous, extending from sites in the lower corona to the interface of the heliosphere with the interstellar medium. The energies of these particles extend from solar wind energies up to ∼10 GeV for ions and ∼100 MeV for electrons. In addition to these heliospheric populations are the galactic cosmic rays (GCR) that penetrate the heliosphere from interstellar space; these particles do not originate in the heliosphere and are described in the companion papers by Helder et al. (2012, this issue) and Schure et al. (2012, this issue). The majority of the observed populations are associated with heliospheric shock waves. However, other populations have no obvious association with shock waves and their acceleration mechanisms are less certain.

Figure 1 is a schematic diagram of the Sun, in the lower left corner, and the heliosphere bounded by the solar wind termination shock and the heliopause, which is the boundary between solar and interstellar plasmas. The energetic particle populations shown are solar energetic particles (SEPs) originating at the Sun, the energetic storm particles (ESP events) associated with the passage of a coronal mass ejection (CME) driven shock wave past the Earth, the corotating energetic ion events associated with the shocks bounding corotating interaction regions (CIRs) in the solar wind, and the anomalous cosmic ray (ACR) component in the outer heliosphere presumably associated with the termination shock. Not shown

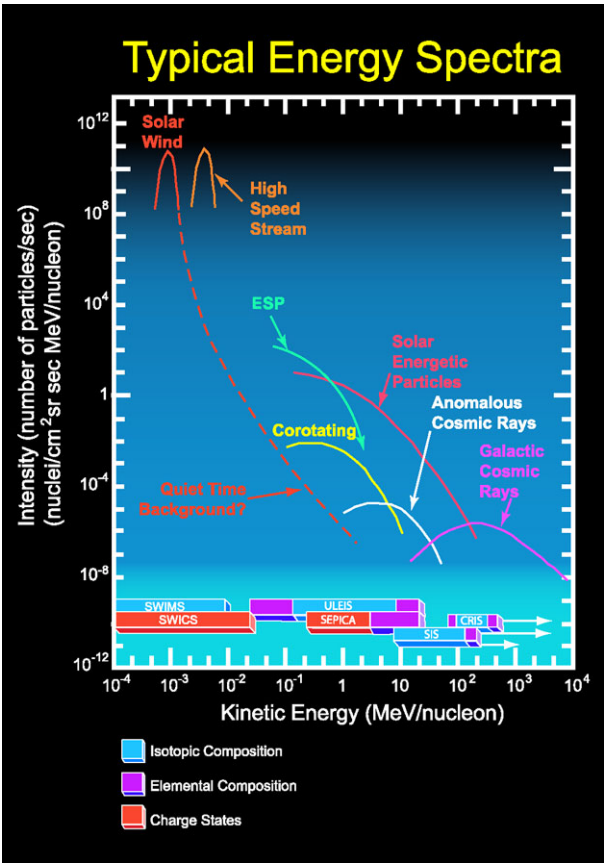

Fig. 2 Schematic diagram of characteristic differential intensity energy spectra for solar wind, energetic storm particles (ESP), solar energetic particles, corotating energetic ion events, anomalous cosmic rays, and galactic cosmic rays (NASA–ACE Brochure, see also Stone et al. 1998). This figure shows the situation in 1997, prior to the launch of ACE. The energy ranges for oxygen covered by the ACE instruments are indicated at the bottom. The fact that there are gaps between the solar wind and ∼0.1 MeV/nucleon regions for various particle components reflects the limitations of earlier measurements

in the figure are the so-called diffuse ions associated with bow shocks at planetary magnetospheres, and the quiet-time suprathermal tails of the solar wind ion distribution functions throughout the heliosphere. Figure 2 is a schematic diagram of the characteristic energy spectra of several of these populations including SEPs, ESP events, corotating energetic ion events, ACRs, GCRs, and the quiet-time suprathermals. Energy spectra of diffuse ions at Earth are not shown but they are typically exponential in energy per charge extending up to ∼ 100 keV/Q. For comparison the energy spectra of the slow and fast solar wind are also shown.

Of these different populations of particles accelerated in the heliosphere, the low-energy ACRs, generally called the termination shock particles (TSPs) with energies less than ∼3 MeV/nucleon, are confined spatially near the solar wind termination shock. The so-called diffuse ions accelerated at planetary bow shocks have nearly isotropic distributions with energies in the range ∼10–100 keV/Q and are confined spatially at planetary bow shocks and are always present. The corotating energetic ion events require that a fast solar wind stream overtake slow wind ahead of it and are known to be associated with enhancements in energetic ions. In contrast, the SEP and ESP events occur as individual events, whose occurrence rate is greatly enhanced during periods of maximum solar flare and CME activity. Figure 3, based on GOES observations of protons with energies greater than 10 MeV, shows how common SEP and ESP events are during solar maximum. The in-

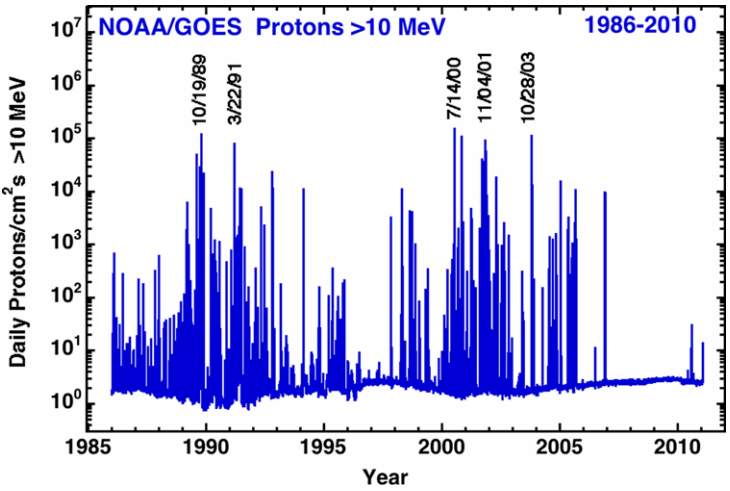

Fig. 3 Daily proton intensity fluences above 10 MeV measured by GOES 6, 7, 8, 11 and 12 during 1986–2010. The increases are solar energetic particle events, the largest of which are indicated. The 11-year solar activity cycle is evident

tensity enhancements of these events during the solar maxima of ∼1991 and ∼2002 provide a distinct contrast with the complete absence of events during the recent deep solar minimum of 2007–2010. At these high energies very few events, if any, are corotating energetic ion events.

The focus of this Chapter is the acceleration of these populations. The basic acceleration mechanisms are few. Nevertheless, the observed features of a particular population generally depend on complexities such as geometry, magnetic field orientation, temporal dependence, specific parameters, seed particle origin, and variability. Although we shall describe the basic acceleration mechanisms with some generality, we shall limit our detailed discussion of the observations and their interpretation to ESP and large SEP events. The other populations are described elsewhere in this volume: the diffuse ions and related field-aligned-beams at Earth's bow shock are described by Burgess et al. (2012, this issue); the smaller so-called impulsive SEP events presumably accelerated by magnetic reconnection processes in flares are presented by Raymond et al. (2012, this issue) and Cargill et al. (2012, this issue); the quiet-time suprathermals are discussed by Fisk and Gloeckler (2012, this issue); finally, the ACRs and their spatial distribution in the boundary regions of the heliosphere are described by Giacalone et al. (2012, this issue).

Most of these populations are associated with, and accelerated by, shocks. Figure 4 shows a result from a study of 19 strong shocks observed by ACE between 1998 and 2003, all with Alfven Mach numbers greater than 3 and compression ratios greater than 2.5. This study is an extension of the investigation described by Giacalone and Jokipii (2012). The plot shows the ratio of the 45–65 keV ion intensity at the shock to that measured one day before shock passage (circles), and the same ratio at randomly selected times during the 4-year period (crosses). Clearly energetic ions in this energy range are enhanced at these strong shocks by a factor of ∼100 most of the time. However, not all shocks have large associated particle intensity enhancements; as will be discussed in Sect. 4, this can result from limited acceleration of solar wind ions with possible additional acceleration of remnant suprathermal/energetic particles. In addition, the predictions of the simplest theory of diffusive shock acceleration at a planar stationary shock do not usually match the observations (van Nes et al. 1984;

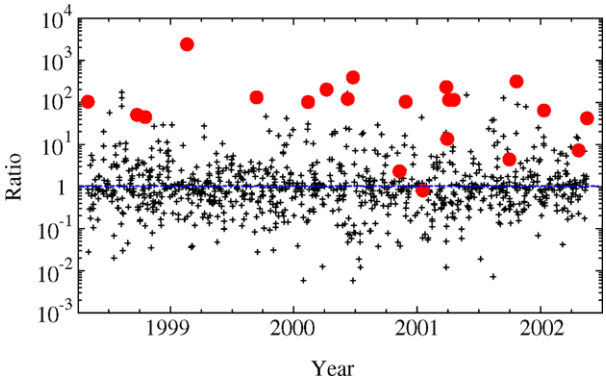

Fig. 4 Ratio of the 45–65 keV ion intensity at shock passage for 19 ESP events at strong shocks to that one day before (*circles*). The *plus signs* are values of the same ratio at randomly selected times for the numerator of the ratio

Lario et al. 2003; Desai et al. 2004). There are also other acceleration mechanisms that are believed to account for some of the populations without obvious shock associations. For example, the quiet-time suprathermals may arise from stochastic acceleration or the "pump mechanism" described by Fisk and Gloeckler (2008). The small, and possibly some of the larger, SEP events may be produced by stochastic acceleration or other processes associated with magnetic reconnection. In Sects. 3 and 4 we shall explore the different mechanisms that operate or may operate in the heliosphere, and the reasons why shock acceleration often produces particle distributions not predicted by the simplest theory.

In Sect. 2 we review the observations of SEP and ESP events, in Sect. 3 we present the basic theory of particle acceleration relevant for the heliosphere, and in Sect. 4 we address extensions of the simplest theory of diffusive shock acceleration that are required to account for interplanetary observations of events associated with shocks.

2 Observations of SEPs and ESP Events

Figure 5 shows GOES measurements of proton differential intensities in six energy channels during the "Haloween" SEP and ESP events of 2003. Five separate particle events are indicated at the bottom of the figure. The vertical red dotted lines indicate the onset times of solar flares with their GOES X-ray class shown at the top of the figure. The vertical black dashed lines indicate the times at which interplanetary shock waves passed Earth orbit. Although this period consists of a complex superposition of five major particle enhancements, eight flares, and seven shocks, the essential temporal structure of SEP and ESP events is apparent. Following a flare at the Sun, events exhibit a rapid onset if they are magnetically well connected to the observer. This SEP phase initially has a large streaming anisotropy away from the Sun, a relatively hard energy spectrum, and a temporal decay timescale of several hours. After ∼1–2 days, in cases where a shock (presumably generated above the flare site) is observed, the event grows in intensity and generally peaks near the shock to form the ESP phase of the event. The ESP phase of the event has a softer energy spectrum than the SEP phase, as is particularly evident in Event 2 starting on 10/28. In that largest event of this period, the SEP phase does not decay but transitions to a very intense ESP phase. In Sects. 2.5 and 3.3 we shall note that ESP phases are often most pronounced in events following closely another event. The first event accelerates particles that provide an enhanced seed particle population for the shock that follows. It is also interesting to note that the SEP phases of the different events in Fig. 5 have very similar maximum intensities, as pointed

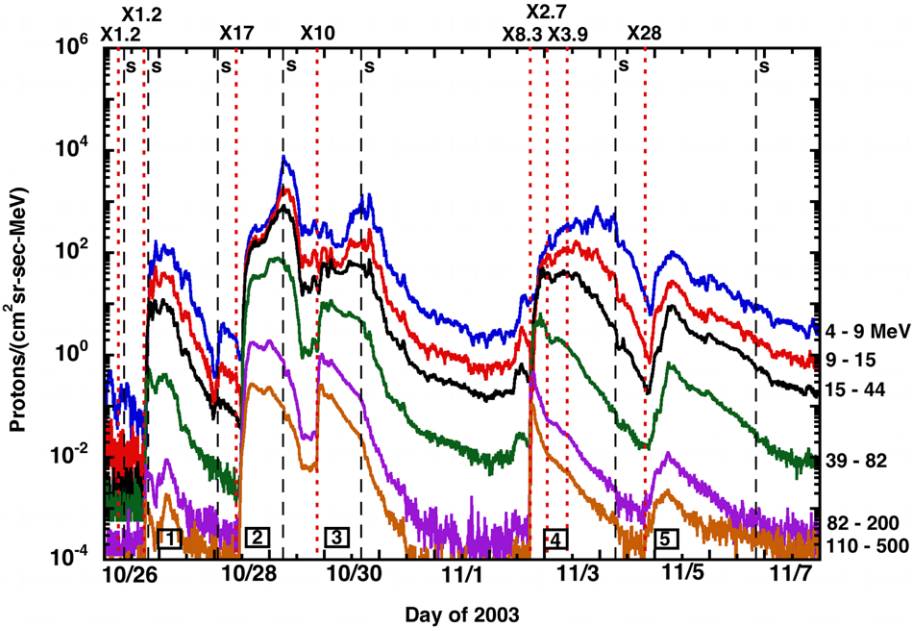

Fig. 5 GOES proton differential intensities during the "Halloween" SEP events. The *numbers at the bottom* identify five identifiable SEP events. The *vertical red dotted lines* indicate the onset times of flares identified above the plot by their GOES X-ray class. The *vertical black dashed lines* indicate the times of interplanetary shocks observed at Earth orbit (from Mewaldt et al. 2005)

out by Reames and Ng (2010). This is particularly evident in the 4 to 9 MeV channel, where the onsets of the 10/28, 10/29, and 11/2 events plateau at a similar intensity level before the onset of the ESP phase. This feature, identified as the "streaming limit" by Reames (1990) (see also Ng and Reames 1994 and Reames and Ng 1998), is due to the regulation of ion escape from the vicinity of the shock by proton-excited waves as described in Sect. 4.2.

2.1 Solar Energetic Particle Composition and Energy Spectra

Although it has long been known that the composition of SEP events is highly variable, Solar Cycle 23 was the first cycle for which there were composition studies of heavy ions in SEP events with good statistical accuracy over a broad energy interval, including resolution of individual elements, isotopes, and ionic charge states. These new capabilities have led to several revisions in understanding the origin of SEP compositional variations.

As an illustration of SEP compositional variability, Fig. 6 (left) shows the relative composition of the 20 largest SEP events of 1997–2005 (as judged by the fluence of >10 MeV protons). All fluence measurements are integrated over as much of the event as possible, starting with the observed onset in each energy interval. Quiet-time background fluences for the same integration periods have been subtracted. In those cases where a new event occurs before the first event is over, the new event period for a given energy interval begins (and the first event ends) when the onset of the new event first causes the overall intensity to increase (see also Mewaldt et al. 2005). Note that the Fe/C ratio in Fig. 6 (left) varies from 0.1 to 10 times the average ratio, and that the lighter elements vary by correspondingly smaller amounts. Breneman and Stone (1985) showed that such variations

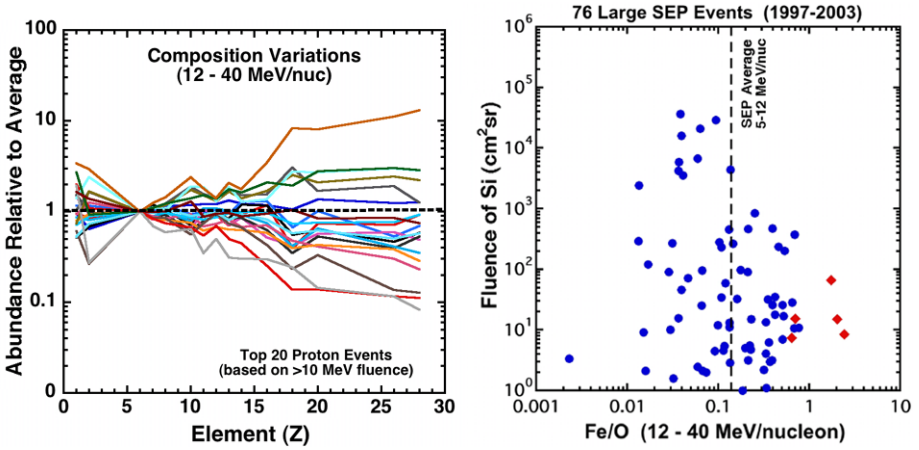

Fig. 6 (*Left*): Relative abundances from H to Ni (normalized to C) in the 20 largest SEP events from 1997 to 2003. (*Right*): Plot of the fluence of Si ($\sim$ midway between O and Fe) versus the Fe/O ratio. Note that the largest events tend to be Fe-poor, while for smaller events there are somewhat more Fe-rich events. The *red points*, which represent events that are believed to be accelerated in impulsive flares, are also enriched in ^{3}He and highly-ionized charge states (see also Mewaldt et al. 2006). Both data sets were measured by the ACE/SIS instrument, with proton data from the EPS sensor on GOES. Also shown is the average 5–12 MeV SEP ratio from Reames (1995)

are organized by the charge-to-mass (Q/M) ratio of the ions, which are not fully stripped for $Z > 2$ (e.g., Klecker et al. 2007). The largest SEP events are typically Fe-poor, while for smaller SEP events there are roughly equal numbers of Fe-rich and Fe-poor events [see Fig. 6 (right)]. Significant variations in the isotopic composition of SEPs (by a factor of up to $\sim$2 in ^{22}Ne/^{20}Ne) can be fit by the same Q/M-dependent relation, showing that these composition variations are rigidity dependent, rather than chemical or nuclear in origin (Leske et al. 2007).

The depletion of Fe and other heavy elements at high energies in some SEP events can be understood by noting that at higher energies the spectra of heavier species typically steepen or "break" at lower energy/nucleon than do the spectra of lighter species. For example, Fig. 7 (left) shows spectra from a 6-hour period following the arrival of the CME-driven shock from the October 28, 2003 event, one of the five large Halloween events shown in Fig. 5. Note in Fig. 7 (right) that the break energies are ordered by the charge–to-mass (Q/M) ratio of the ions [the mean charge states were measured in the same event at higher energy than the "break" energy by the MAST/SAMPEX instrument using the geomagnetic method]. Such Q/M-dependent spectral breaks are a common feature in large SEP events (Tylka et al. 2000; Cohen et al. 2005; Mewaldt et al. 2005).

This behavior can be explained if the spectra break at the same value of the diffusion coefficient as SEP ions escape the shock during acceleration (Cohen et al. 2005; Mewaldt et al. 2005). For typical rigidity-dependent diffusion coefficients, Fe spectra will break at lower energy/nucleon than lighter ions because Fe has a higher rigidity than lighter ions at the same energy/nucleon. Li et al. (2005) predicted that for quasi-parallel shocks the break-energy per nucleon would scale as $(Q/M)^s$ with $s \approx 2$, which is close to the observed dependence in Fig. 7 (right). However, Li et al. (2009) later showed that values between $s \approx 0.2$ (for a quasi-perpendicular shock) and $s \approx 2$ were possible depending on the magnetic obliquity of the shock and other conditions. It is hoped that multi-spacecraft studies during

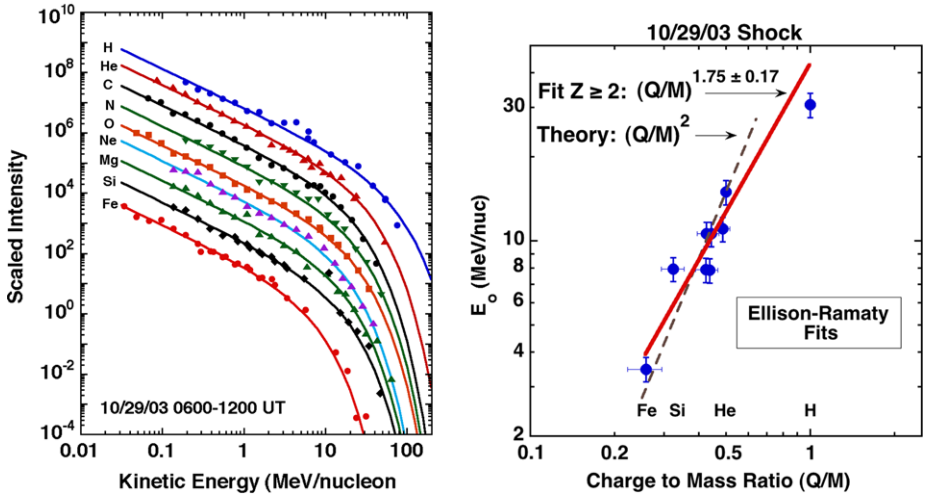

Fig. 7 (*Left*): Energy spectra from ACE and GOES during the 6-hour period following a shock on 29 October 2003 are fit with the Ellison-Ramaty (1985) spectral form for differential intensity, $J = CE^{-\gamma}\exp(-E/E_0)$, all with $\gamma = 1.3$ (Mewaldt 2007). Elements have been multiplied by scale factors to separate the spectra. (*Right*): The E_0 values determined from the left panel are plotted versus measured Q/M values. Fits to the $Z \geq 2$ data give a $(Q/M)^{1.75}$ dependence, similar to, but somewhat weaker than expected from, the theory of Li et al. (2005)

Solar Cycle 24 with STEREO and L1 spacecraft that include ACE, SOHO and Wind will test ideas about the role of shock geometry in shaping SEP composition and energy spectra.

The Fe-rich SEP events in Fig. 6 typically also have other unusual properties, including enrichments in ^{3}He and highly-ionized charge states of Fe and other heavy elements (Cohen et al. 1999a; Mewaldt et al. 2006; Desai et al. 2006a). There have been several proposed explanations for these compositional features, including the acceleration of remnant seed-particles from earlier small ^{3}He-rich "impulsive" events (Mason et al. 1999b; Tylka et al. 2005; Mewaldt et al. 2006; Tylka and Lee 2006), mixtures of flare and shock-accelerated ions (e.g., Cane et al. 2003, 2006); shock acceleration of a mixture of solar wind and escaping flare particles (Li and Zank 2005a), and the acceleration of a mixture of suprathermals and ICME material (Mewaldt et al. 2007; Li et al. 2012). While all of these may occur, in our opinion there is more direct evidence to support the first of these explanations (acceleration of remnant suprathermal ions) as evidenced by the ubiquitous presence of suprathermal ^{3}He in interplanetary space at 1 AU (Mason et al. 1999b; Wiedenbeck et al. 2003) and by the frequent overabundance of ^{3}He in gradual SEP events (Cohen et al. 1999a; Desai et al. 2006a; Mewaldt et al. 2006).

2.2 Solar Energetic Particles, CMEs, and Flares

A variety of evidence has shown that the Sun can accelerate particles to high energy in at least two ways. In large solar flares X-ray and γ-ray data show that particles can be quickly accelerated to GeV energies in the low corona (see, e.g., reviews by Lin 2011 and Raymond et al. 2012, this issue). The energy released in large flare events that is ultimately responsible for particle acceleration is understood to be due to the reconnection of opposing magnetic fields. It appears that most of the flare-accelerated particles in these events lose their energy in the solar atmosphere and do not escape the Sun. Reconnection events also happen on

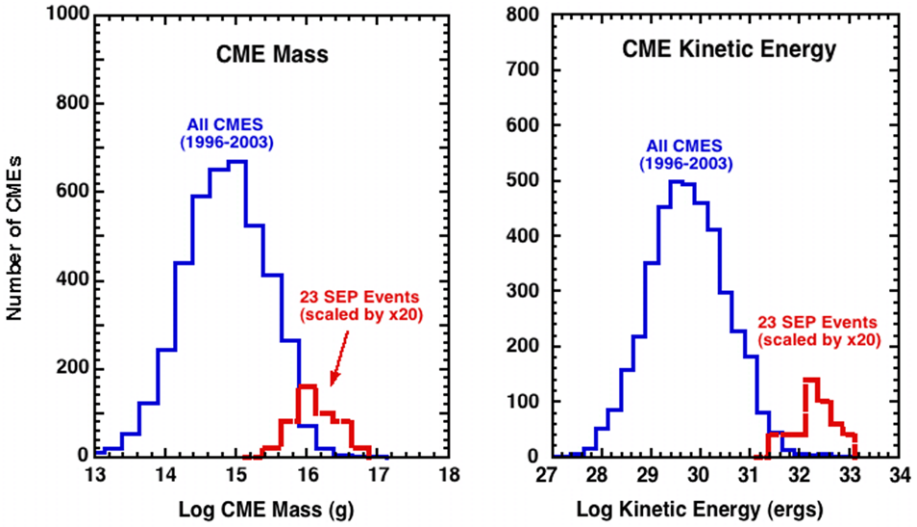

Fig. 8 (*Left*) A histogram of all CME masses from 1997–2003 (Gopalswamy 2006) is compared to the mass of CMEs associated with 23 of the 50 largest SEP events of Solar Cycle 23 (scaled up by × 20). (*Right*) Here the 1997–2003 CME kinetic energy distribution is compared to the kinetic energy of CMEs associated with the same 23 large SEP events (from Mewaldt et al. 2008)

much smaller scales and it is estimated that there are ∼10,000 small particle-acceleration events per year that can be observed at 1 AU in sub-MeV electrons and ions (Wang et al. 2012; Raymond et al. 2012, this issue). On the other hand, most of the largest SEP events observed at Earth are associated with large, fast CMEs, and are widely (but not universally) believed to be due to shock acceleration processes. The number of these events observed near Earth per year at solar maximum is ∼10 to 20 (see, e.g., the list in Cane et al. 2006).

2.3 Solar Energetic Particles and CME Properties

Several authors have shown that there is a correlation between the peak intensity of SEPs and CME speed (Reames 2000; Kahler 2001), as might be expected from the theory of shock acceleration (see Sect. 3.2). However, the peak intensity of SEPs associated with a given CME speed varies over ∼4 orders of magnitude, suggesting that there are also other important variables that determine accelerated particle intensities.

A comparison of the CME speeds associated with the 50 largest SEP events of Solar Cycle 23 (based on the fluence of >30 MeV protons measured by GOES) shows that most of the events are associated with fast CMEs having velocities >1500 km/s, although a few have speeds as low as 700–800 km/s. Shown in Fig. 8 (left) and 8 (right) are comparisons of the CME mass and kinetic energy for all CMEs with those for the largest SEP events. It is clear that large SEP events require massive CMEs—those with 10^{15} g or more. Previous studies have shown that the largest SEPs are associated with "wide" CMEs (Kahler et al. 1984), and, of course, wide CMEs are generally more massive [Note that estimates of SEP kinetic energies and of CME speed, mass, width, and other properties have uncertainties that depend to some extent on where they are observed from (see e.g., Emslie et al. 2004)]. Figure 8 (right) indicates that the CME property that best isolates the largest SEP events is CME kinetic energy. All of the top 50 SEP events for which there are kinetic energy

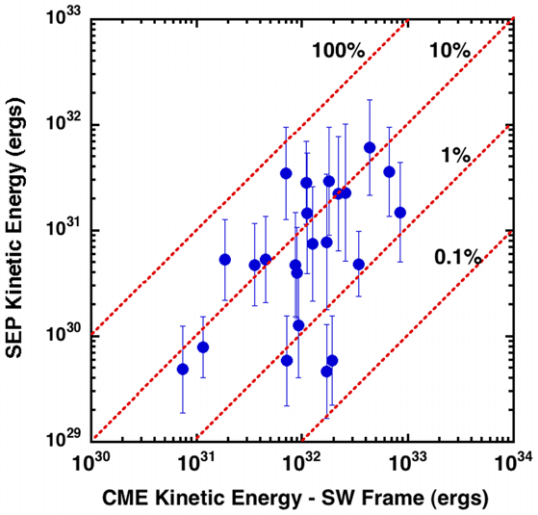

Fig. 9 The measured kinetic energy of 23 large SEP events from Solar Cycle 23 is plotted versus the CME kinetic energy (from Mewaldt et al. 2008). SEP fluence spectra were measured by instruments on ACE, SAMPEX and GOES from ∼0.03 to ∼400 MeV per nucleon, and corrected for the source location and transport effects as described in the text. The CME kinetic energies were measured by the LASCO instrument on SOHO (see e.g., Ontiveros and Vourlidas 2009). At the time of this study in early 2008 these were the only events of the top 50 SEP events for which CME kinetic energies were available

measurements available had CME kinetic energies $>3 \times 10^{31}$ ergs, a property shared by only ∼2 % of all CMEs from 1996–2003 (Mewaldt et al. 2012).

In an interdisciplinary study, Emslie et al. (2004) combined a wide range of imaging and *in situ* data to measure the energy budget of two large SEP events, April 21, 2002 and July 23, 2002. Included were estimates (and uncertainties) for the CME, thermal plasma at the Sun, hard X-rays produced by accelerated electrons, γ-ray producing ions, and solar energetic particles (a later paper by Emslie et al. 2005 gave revised estimates of flare thermal energies and also estimated the total irradiated energy in the two events). The best estimates of the various components indicated that the CME contained the greatest fraction of the released energy in both events.

One interesting result of the Emslie et al. (2004) study was that the estimated kinetic energy in accelerated particles (protons, electrons, and heavy ions) observed at 1 AU in the April 21, 2002 event was ∼15 % of the CME kinetic energy. Later studies including more SEP events found considerable spread, with a typical SEP/CME kinetic energy ratio of ∼5 %–10 % (Mewaldt et al. 2005; Mewaldt 2007). In Fig. 9 we compare the SEP/CME kinetic energy ratio for 23 of the Top 50 SEP events of Solar Cycle 23 [all events for which CME kinetic energy estimates were available at that time (Mewaldt et al. 2008)]. These estimates take into account the longitude distribution of SEPs, the fact that SEPs diffuse and cross 1 AU multiple times, increasing their chance to be observed, and adiabatic energy loss due to pitch-angle scattering in the diverging interplanetary magnetic field. In addition, they compare the CME and SEP kinetic energies in the rest frame of the solar wind. Note that while there is considerable scatter, and the uncertainties are large, on average ∼5 %–10 % of the CME kinetic energy apparently goes into accelerating energetic particles. It is interesting that a similar acceleration efficiency is required of supernova shocks if they are to keep the Galaxy filled with galactic cosmic rays over their ∼15 million year lifetime (e.g., Ptuskin 2001).

2.4 What Do CME-Driven Shocks Accelerate?

Solar Cycle 23 was the first for which there were comprehensive composition and energy spectra measurements in the energy range from ∼40 keV/nuc to ∼1 MeV/nuc. Fig-

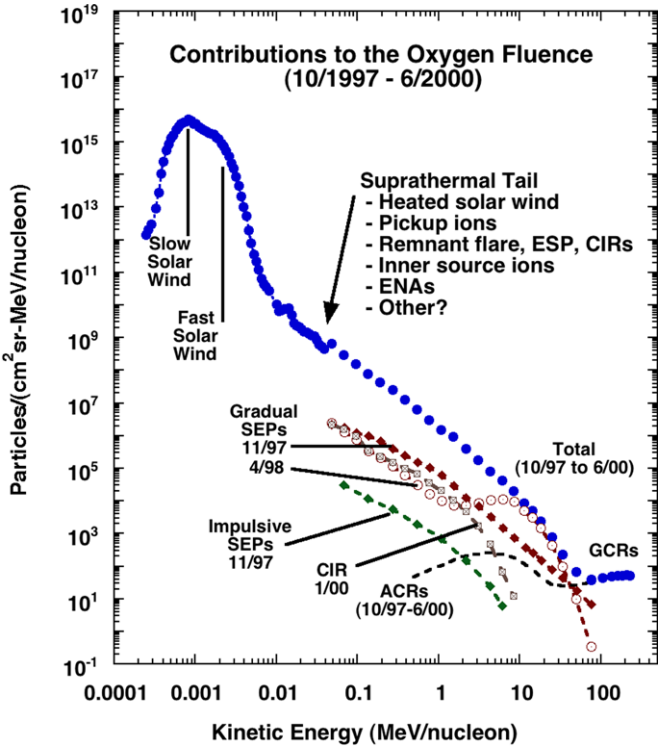

Fig. 10 Fluence of oxygen nuclei measured from October 1997 to June 2000 by instruments on ACE (adapted from Mewaldt et al. 2007). Also shown are examples of solar and interplanetary contributions to the fluence spectrum, and a list of sources that contribute to the suprathermal tail region, which serves as the primary source of seed particles for acceleration by CME-driven shocks

ure 10 illustrates some of the many sources that contribute to an evolving pool of ∼0.01 to ∼1 MeV/nucleon suprathermal ions in the inner solar system. These include particles accelerated in small impulsive flares, typically enriched in heavy elements up to Fe and beyond and in ^{3}He (e.g., Mason et al. 2004); interstellar pickup ions (Gloeckler et al. 1994), inner-source pickup ions (Geiss et al. 1995), CIRs (Desai et al. 2006b), and earlier large SEP events (Mewaldt et al. 2006). The composition of this pool of suprathermal ions has been found to vary over the solar cycle (Desai et al. 2006b). In addition to the known sources of suprathermal ions at 1 AU, there are suggestions that more exotic sources may make significant contributions, including energetic neutral atoms (ENAs) from the heliosheath (Chalov and Fahr 2003; Schwadron and McComas 2010; Bochsler and Möbius 2010) and Sun-grazing comets (Gloeckler et al. 2000a; Bzowski and Krolikowska 2005; Neugebauer et al. 2007). Finally, the ubiquitous presence of suprathermal tails (e.g., Gloeckler et al. 2000b, 2000c) has also led to suggestions as to how ions can be accelerated more or less continuously in interplanetary space (e.g., Fisk and Gloeckler 2008; Jokipii and Lee 2010).

Although it had earlier been assumed that CME-driven shocks accelerate mainly solar wind, it was shown that the composition of large SEP events differs in systematic ways from the solar wind composition, including, e.g., depletions of C, Ne and S (Mewaldt et al. 2006). In addition, many large SEP events are found to have large admixtures of species that are rare

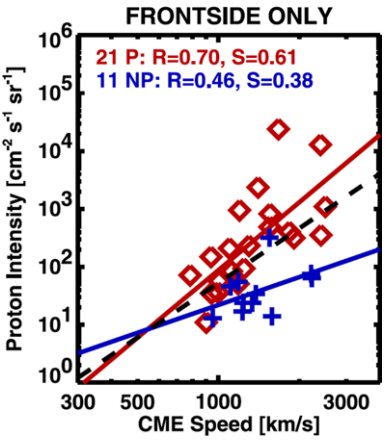

Fig. 11 Peak proton intensity versus CME speed for SEP events with a preceding frontside CME (P; *red diamonds*) and for no preceding CME (NP; *plus symbols*) from Gopalswamy et al. (2004). *Solid lines* are the regression lines for the P and NP groups. The *dashed regression line* is for all data points

in the solar wind but present in the suprathermal pool, including ^{3}He (Cohen et al. 1999a; Mason et al. 1999b), He^+ (Kucharek et al. 2003), and highly-ionized charge states of Fe (Mazur et al. 1999; Cohen et al. 1999b; Tylka et al. 2001; Klecker et al. 2007). Theoretical studies also show that suprathermal ions are much more easily injected into the acceleration process (see Sect. 4.3).

2.5 Pre-conditioning by Previous CMEs

Statistical studies of Solar Cycle 23 SEP events suggest that CMEs that erupt soon (within $<$24 hours) after a previous CME from the same source region are much more efficient in accelerating particles than those erupting into a pristine environment (Gopalswamy et al. 2004; see Fig. 11). Li and Zank (2005b) suggested that enhanced turbulence levels following the first shock lead to more efficient acceleration and reported model calculations suggesting that particles could be accelerated to $\sim$30 times higher energy at the second shock. It is also possible that the higher intensities associated with the second shock are due to a larger population of suprathermal seed particles (Gopalswamy et al. 2004). Mewaldt et al. (2012) supported this idea by noting that Helios observations show a reservoir of accelerated particles downstream of CME shocks that decay gradually with e-folding times of 8 to 16 hours (Reames et al. 1997b). This source of pre-accelerated seed particles could be a key factor in causing the higher intensities associated with the second of two CME shocks.

Li et al. (2012) suggested a two-CME scenario associated with a pseudo-streamer-like configuration in which reconnection between closed magnetic field lines that drape the preceding CME and open field lines draping the subsequent CME lead to an enhanced seed population and higher turbulence levels. Other suggested explanations for the observations include differences in the open and closed field-line geometry, and a lowering of the Alfven velocity, leading to the formation of a stronger shock (Gopalswamy et al. 2004). All of these suggestions could benefit from additional modeling of the processes involved, and from in situ observations of conditions closer to the Sun in the wake of CMEs, as expected from Solar Probe Plus and Solar Orbiter near the end of this decade.

2.6 Energetic Neutral Atoms—A New Window into SEP Acceleration Processes

In December, 2006, four X-class flares provided the final fireworks of Solar Cycle 23 just after the launch of NASA's twin STEREO spacecraft. The first of these events, an X9 flare

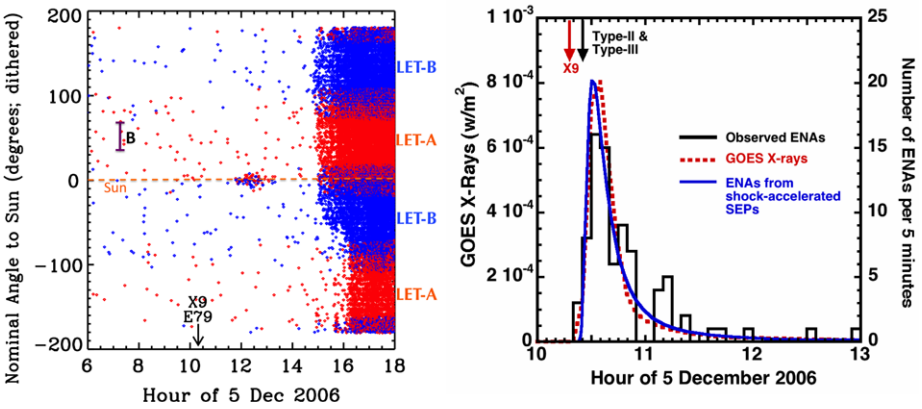

Fig. 12 (*Left*) Measured angle to the Sun for individual 1.6–12 MeV protons observed on December 5, 2006 by the STEREO Low Energy Telescopes (*Red* = LET sensor on STEREO-A; *blue* = Stereo-B; see Mewaldt et al. 2009). Note the group of events that arrived from within ±10° of the Sun between ∼1130 UT to ∼1350 UT, well before the SEP onset at ∼1445 UT. The range of magnetic field orientations connecting to the Sun between 1130 and 1350 UT is shown as a bar. The X9 flare onset is also indicated. It was concluded that these particles must have been ENAs. (*Right*) The derived emission profile of the ENA burst in the left panel is compared with the GOES 1–8 Å X-ray profile, and with a profile derived from SEPs assumed to be accelerated by an 1800 km/s CME launched at the onset of the X-ray flare (Mewaldt et al. 2010)

at E79°, was magnetically poorly connected to Earth, and the first >30 MeV protons did not arrive until several hours later. However, there was a low-energy (∼2–12) MeV precursor consisting entirely of protons that began arriving within the first hour. Surprisingly, essentially all of the particles in this precursor arrived from within ±10° of the Sun (see Mewaldt et al. 2009 and Fig. 12).

After considering alternatives, it was concluded that the precursor was made up of energetic neutral H atoms (ENAs). The measured kinetic energies were used to calculate the ENA emission profile from the Sun as shown in Fig. 12. Note that the ENA emission profile is consistent with the soft X-ray time profile, suggesting that the ENAs were due to the charge exchange of flare-accelerated particles. This is certainly one possibility, but it requires that a significant fraction of the flare-accelerated protons make it into the high corona, or else the ENAs would be stripped before leaving the Sun. This conclusion is based in part on the estimated number of flare-accelerated protons derived from RHESSI γ-ray observations.

A second possibility illustrated in the right panel of Fig. 12 is that the ENAs could be produced by charge exchange of protons accelerated by the CME-driven shock (assuming CME properties typical of large SEP events—see Mewaldt et al. 2010). Note that there was a type-II radio burst in this event, indicating that a shock formed, but unfortunately there were no coronagraph observations to further test this possibility.

The discovery of ENAs associated with large solar events opens up a new window into SEP acceleration and transport that can reveal when, where, and how low-energy solar protons are accelerated, interact with coronal material, and escape from the Sun.

2.7 Ground Level Solar Energetic Particle Events

Ground-Level Events (GLEs) are SEP events that are detected by neutron monitors (e.g., Lopate 2006), muon detectors (e.g., Falcone et al. 2003) or ground-based ionization chambers (e.g., Forbush 1946). Solar Cycle 23 included the largest GLE in ∼50 years: the

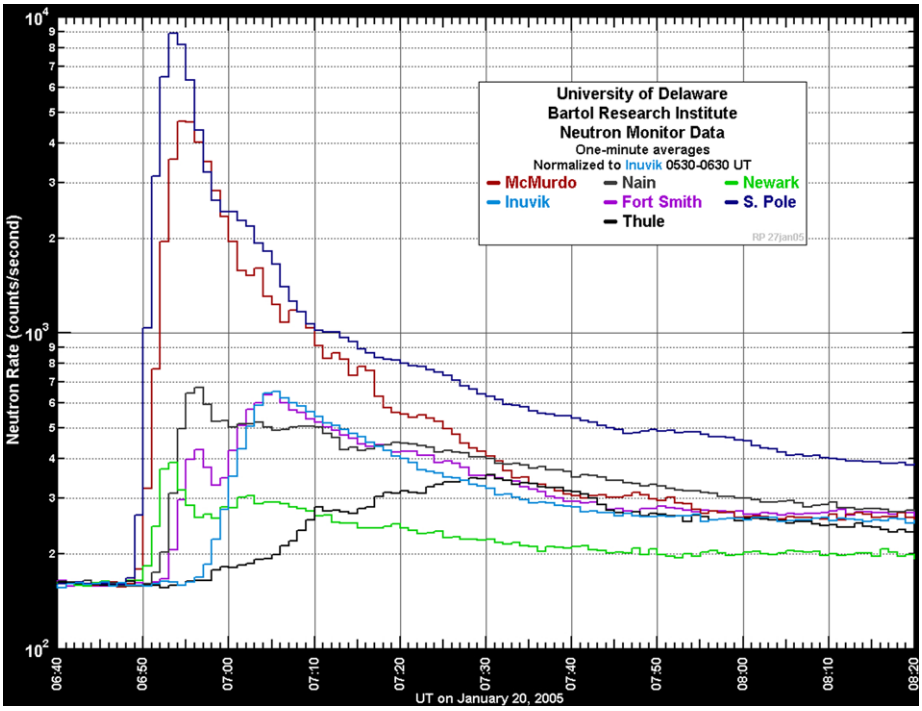

Fig. 13 The January 20, 2005 GLE was the largest observed at sea level since the famous February, 1956 GLE, the largest ever recorded. The January 20 event was especially intense at South Pole and McMurdo, Antarctica. Also shown are five other neutron monitors. Figure furnished by the University of Delaware Bartol Research Institute (http://neutronm.bartol.udel.edu/gle2005.html)

January 20, 2005 event, during which the count rate at the McMurdo neutron monitor in Antarctica reached ∼30 times the cosmic-ray background in a few minutes (see Fig. 13). This event also produced the second highest >100 MeV count rate in 35 years of NOAA's GOES satellites (Kunches 2005). There is considerable debate about how the high-energy particles in this event were accelerated so rapidly (e.g., McCracken et al. 2008; Masson et al. 2009). However, it should be noted that the CME characteristics were also very extreme—Gopalswamy et al. (2012) estimate the CME sky-speed at 3675 km/s, the fastest on record. The fluence spectra of all sixteen ground level events during Solar Cycle 23 were found to be best fit by double power-law spectra such as those in Fig. 14. Ground-level events also tend to be Fe-rich at energies >20 MeV/nuc (Tylka et al. 2005; Mewaldt et al. 2012).

Recently, there has been considerable progress in deriving the rigidity spectra of GLE events from neutron monitor data. Tylka and Dietrich (2009) have collected neutron monitor and spacecraft data from NOAA's GOES satellites for most of the GLE events since 1976. They find that the integral rigidity spectra of GLE events can be fit with the double-power-law formulation shown in Fig. 15. Thus, the largest SEP events have two spectral breaks. The lower energy one at proton energies of ∼5 to ∼50 MeV has been interpreted as due to rigidity-dependent escape from the CME-driven shock (Vainio 2003; Cohen et al. 2005; Mewaldt et al. 2005; Li et al. 2009), while the spectral break at ∼1 GV presumably reflects some additional limitation of the acceleration process.

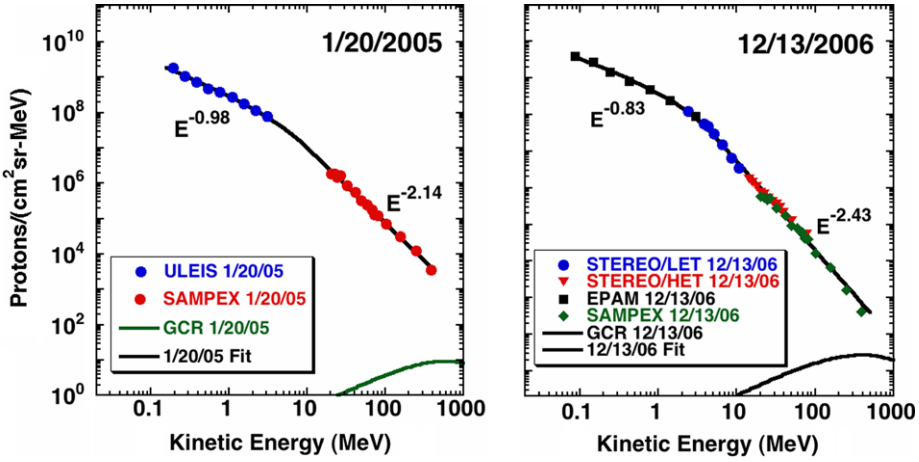

Fig. 14 Proton energy spectra for the last two of the 16 ground-level events of Solar Cycle 23 based on data from the ACE, SAMPEX, STEREO, and GOES-8 missions (from Mewaldt et al. 2012). In each case the spectra are fit by the double power-law spectrum of Band et al. (1993). Both of these events have rather hard spectra above the break; slopes for the 16 GLE events of Solar Cycle 23 ranged from −2.1 to −4.5. The galactic cosmic ray proton fluence during these events is also indicated

2.8 Future Prospects

The combination of STEREO and near-Earth spacecraft are now providing a 360° view of the Sun and interplanetary medium. This combination should be able to address the questions of the relative contributions of flare and shock-accelerated particles in large SEP events, the importance of shock geometry, and issues of how particles are transported in longitude.

In 2017 and 2018 the Solar Orbiter and Solar Probe Plus missions will be launched and begin their journeys to the inner heliosphere, providing the opportunity to explore particle acceleration in situ within the prime acceleration region of CME-driven shocks (down to 9.5 solar radii), and close to the source of many of the populations of suprathermal seed particles. These new missions, aided by imaging and modeling, will directly or indirectly address most, if not all, of the issues presented here.

3 Basic Physical Processes and Theories of Particle Acceleration

On the timescales and lengthscales for the acceleration of the energetic particle populations described in Sect. 1 the coronal and heliospheric plasmas are approximately collisionless. Therefore, the acceleration is due to the electric field arising from the charge and current distribution in the plasma averaged over the spacing of the discrete particles. In most cases the acceleration processes operate on the magnetohydrodynamic (MHD) timescales and lengthscales, over which the electrical conductivity is large enough that

$$\mathbf{E}+\delta\mathbf{E} = -c^{-1}\left[(\mathbf{V}+\delta\mathbf{V})\times(\mathbf{B}+\delta\mathbf{B})\right] \simeq -c^{-1}(\mathbf{V}\times\mathbf{B}) - c^{-1}\left[(\delta\mathbf{V}\times\mathbf{B})+(\mathbf{V}\times\delta\mathbf{B})\right], \quad (1)$$

where $\mathbf{E}$, $\mathbf{V}$ and $\mathbf{B}$ are the electric field, plasma velocity and magnetic field averaged over the MHD fluctuations, and $\delta\mathbf{E}$, $\delta\mathbf{V}$ and $\delta\mathbf{B}$ are the fluctuating values.

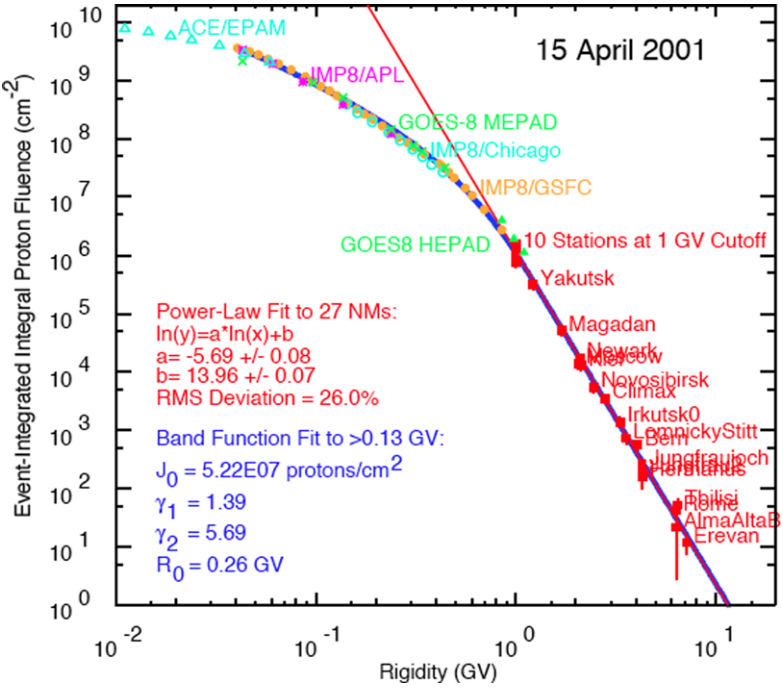

Fig. 15 Integral rigidity spectrum of the 15 April 2001 GLE as measured by the world-wide neutron monitor network and lower energy space instruments (Tylka and Dietrich 2009). The data with >0.13 GV (10 MeV) are fit with the function of Band et al. (1993) using the parameters shown in blue. Note the spectral break at ∼1 GV, corresponding to a proton kinetic energy of ∼440 MeV. While there are inevitable uncertainties involved in combining ground-based and spacecraft data from a variety of sources (e.g., Adriani et al. 2011), this appears to be the most promising such effort to date

The first term on the right hand side of Eq. (1) is the electric field due to the bulk motion of the plasma. If the bulk velocity is nearly uniform then we may transform to that frame of reference in which $\mathbf{V} = 0$, and therefore, due to this term, $\mathbf{E} = 0$. In order to obtain particle acceleration (or deceleration) from this term $\mathbf{V}$ must vary. Thus, acceleration by this term is intimately connected to the spatial and temporal structure of $\mathbf{V}$ as recognized by Fermi (1949, 1954). $\mathbf{V}(\mathbf{x}, t)$ may vary coherently and systematically or stochastically, leading to both first-order and second-order Fermi acceleration. The second term on the right hand side of Eq. (1) is the electric field due to the MHD fluctuations $\delta\mathbf{V}$ and $\delta\mathbf{B}$. A broad spectrum of waves or turbulence leads inherently to a stochastic vector field $\delta\mathbf{E}(\mathbf{x}, t)$ and a version of stochastic or second-order Fermi acceleration.

Of course, the actual acceleration process depends not only on the structure of $\mathbf{V}(\mathbf{x}, t)$ or $\delta\mathbf{E}(\mathbf{x}, t)$, but also on the transport of the accelerating particles. For example, even if $\mathbf{V}(\mathbf{x}, t)$ is inhomogeneous, acceleration according to the first term on the RHS of Eq. (1) is impossible if the particles do not have access to the regions of inhomogeneity. In principle transport is governed by the Vlasov (or collisionless Boltzmann) equation. In practice, however, even with the help of modern computers, progress is limited without further simplifications. Most of the particle populations described in Sect. 1 are characterized by speeds $v \gg |\mathbf{V}|$, by nearly isotropic distributions, and by spatial scales larger than pitch-angle scattering mean free paths. There are of course exceptions; for example, early in SEP events, particles are observed to stream away from the Sun with high anisotropy. As another example, the ve-

locities of particles extracted and accelerated out of the solar wind cannot satisfy $v \gg |\mathbf{V}|$. Nevertheless, these generally observed simplifications provide a valuable place to start in describing the transport of energetic particles in the heliosphere.

3.1 The Transport Equation of Parker

Parker (1965) employed these approximations mentioned above in deriving the energetic particle transport equation

$$\frac{\partial f}{\partial t} + (\mathbf{V} + \mathbf{V}_D) \cdot \nabla f - \nabla \cdot \mathbf{K} \cdot \nabla f - \frac{1}{3}(\nabla \cdot \mathbf{V}) p \frac{\partial f}{\partial p} - \frac{1}{p^2} \frac{\partial}{\partial p} \left(p^2 D \frac{\partial f}{\partial p} \right) = R, \quad (2)$$

where $f(p, \mathbf{x}, t)$ is the omnidirectional distribution function of a particular particle species, p is particle momentum magnitude, $\mathbf{K}(p, \mathbf{x}, t)$ is the spatial diffusion tensor, $D(p, \mathbf{x}, t)$ is the momentum diffusion coefficient for nearly isotropic distributions, $R(p, \mathbf{x}, t)$ is a source or injection rate, and $\mathbf{V}_D(p, \mathbf{x}, t)$ is the drift velocity given by

$$\mathbf{V}_D = \frac{pvc}{3Q} \nabla \times \frac{\mathbf{B}}{B^2}, \quad (3)$$

where Q is particle charge and c is the speed of light. Evidently Eq. (2) expresses particle conservation under the transport processes of advection $\mathbf{V}$, drift $\mathbf{V}_D$, spatial diffusion $\mathbf{K}$, compression $(\nabla \cdot \mathbf{V})$, momentum diffusion D, and injection R. Interestingly $\mathbf{E}$ does not appear explicitly in Eq. (2). Under the approximations employed, the acceleration is entirely described by the terms involving the p-derivatives. The first of these terms depends only on $(\nabla \cdot \mathbf{V})$. Included in this term are first-order and second-order Fermi acceleration due to variations in the bulk flow, and the drift transport of particles parallel to the electric field given by the first term on the RHS of Eq. (1). The second of these terms describes stochastic acceleration of particles due to an incoherent superposition of MHD fluctuations with electric fields given by the final term in Eq. (1). Actually this last term on the LHS of Eq. (2) was not included by Parker (1965) but was introduced subsequently by many authors to describe different versions of stochastic acceleration (e.g. Lee and Völk 1975).

A systematic expansion $[(\nabla \cdot \mathbf{V}) > 0]$ gives rise to systematic deceleration. A heliospheric example is the adiabatic deceleration of GCRs in the solar wind, a process that motivated Parker to develop Eq. (2) in the first place. Similarly, an isolated compression $[(\nabla \cdot \mathbf{V}) < 0]$ gives rise to systematic acceleration. If the spatial scale of the convective-diffusive gradient is smaller than the spatial scale of the compression, then the energy gain is adiabatic (Drury et al. 1982). However, if the reverse is true, as is generally the case at a shock, then spatial diffusion allows some particles to traverse the shock many times. These particles sample the compression many times and are accelerated to high energies. This is the essence of diffusive shock acceleration (DSA) (Krymsky 1977; Axford et al. 1977; Bell 1978; Blandford and Ostriker 1978).

3.2 Planar Stationary Diffusive Shock Acceleration

The simplest configuration to illustrate the process of diffusive shock acceleration is a planar stationary shock with particle injection R from the ambient plasma into the process of shock acceleration at the shock front. To illustrate the application of DSA to ESP and gradual SEP events, we modify this configuration in two ways: Firstly we replace R, which we set equal

to zero, by specifying $f(p, z \to \infty) = f_\infty(p)$, where z is the coordinate measuring distance upstream of the shock. Secondly we replace the variable z upstream of the shock by

$$\zeta(z) = \int_0^z dz' V\big[K_{zz}(z')\big]^{-1}, \tag{4}$$

where $V_z(z > 0) = -V$. If $K_{zz}(z)$ increases sufficiently rapidly as $z \to \infty$ that $\zeta(z \to \infty) = \zeta_\infty$, then the configuration has a "free escape boundary" that allows particles to escape the shock in the upstream direction. This generalization is not strictly valid for a stationary configuration since the variable upstream diffusion coefficient would create temporal variation at the shock. Nevertheless it captures the effect of magnetic mirroring upstream of the shock (particles are repelled away from the shock against pitch-angle scattering at the outer edge of the foreshock) and accounts for the observed escape of particles upstream of the shock early in SEP events. Both modifications are crucial in applying DSA to ESP and gradual SEP events.

In Eq. (2) we take $\partial f/\partial t = 0$ and $D = 0$, and we ignore $\mathbf{V}_D$, since it does not affect the distribution in planar geometries. With $V_z(z < 0) = -V_d$, we obtain $dV_z/dz = -(V - V_d)\delta(z)$. Integrating this simplified version of Eq. (2) we obtain

$$f(p, z > 0) = f_0 - (f_0 - f_\infty)\big[1 - \exp(-\zeta)\big]\big[1 - \exp(-\zeta_\infty)\big]^{-1}, \tag{5}$$

$$f_0(p) = \beta \int_0^p \frac{dp'}{p'} f_\infty(p')\big[1 - \exp\big(-\zeta'_\infty\big)\big]^{-1}\left(\frac{p}{p'}\right)^{-\beta} \exp\left[-\beta \int_{p'}^p \frac{dp''}{p''} \frac{\exp(-\zeta''_\infty)}{[1 - \exp(-\zeta''_\infty)]}\right], \tag{6}$$

where $f_0(p)$ is the distribution function at and downstream of the shock, $\zeta'_\infty = \zeta_\infty(p')$, $\zeta''_\infty = \zeta_\infty(p'')$, $\beta \equiv 3X(X-1)^{-1}$, and $X(\equiv V/V_d)$ is the plasma compression ratio at the shock. The flux of particles in the solar wind frame far upstream of the shock is given by

$$-K_{zz}\frac{\partial f}{\partial z}\bigg|_{z\to\infty} = V(f_0 - f_\infty)\frac{\exp(-\zeta_\infty)}{[1 - \exp(-\zeta_\infty)]} \tag{7}$$

We first ignore our two modifications to the standard planar stationary configuration of DSA introduced for ESP and gradual SEP events. This is accomplished by taking $\zeta_\infty(p) \to \infty$, so that there is no free escape boundary, and by setting $f_\infty(p) \propto \delta(p - p_0)$, so that particles are injected out of the upstream plasma at the shock into the acceleration process presumably at momentum $p_0 \cong MV$, where M is particle mass. Care must be exercised in this case with the identification of $f_\infty(p)$. Since $v \gg V$ is not satisfied, the theory of DSA is not able to treat the injection process or rate with rigor. Most of the incident upstream plasma particles are heated at the shock, but continue downstream and are not able to participate in DSA. Normally only a fraction of them, less than 1 % of the number density (e.g. Lee 1982 and Gordon et al. 1999), is able to participate in DSA. We shall return to the issue of injection in Sect. 4.3. Ignoring the two modifications, Eqs. (5)–(7) yield

$$f(p > p_0, z > 0) = f_0 \exp(-\zeta), \tag{8}$$

$$f_0(p) \propto (p/p_0)^{-\beta}, \tag{9}$$

$$-K_{zz}(\partial f/\partial z)\,|_{z\to\infty} = 0. \tag{10}$$

Equations (8)–(10) reveal the essential well-known properties of DSA: the power-law index $-\beta$; the upstream exponential decay of the accelerated particles due to the balance between

shockward advection and anti-shockward diffusion; and the absence of upstream particle escape. Equation (9) demonstrates why particle differential intensity correlates with CME speed; if the constant of proportionality, which is proportional to the particle injection rate, is not sensitive to shock strength, then X clearly increases with CME speed and β decreases so that the spectrum hardens and results in increased intensity at all energies. Thus, in this case, peak intensity occurs at the shock, is linearly dependent on the injection rate, and more sensitively dependent on the injection speed and the shock compression ratio.

For the stationary planar configuration described by Eqs. (8)–(10), the corresponding time-dependent case, in which steady injection commences at $t = 0$, yields the characteristic time for particles to be accelerated to momentum p as (Axford 1981; Forman and Drury 1983; Drury 1983)

$$\tau_a = \frac{\beta}{V}\int_{p_0}^{p}\frac{dp'}{p'}\left(\frac{K_{zz,u}(p')}{V}+\frac{K_{zz,d}(p')}{V_d}\right), \tag{11}$$

where $K_{zz,u}(p)$ and $K_{zz,d}(p)$ are the upstream and downstream diffusion coefficients, respectively. The acceleration time τ_a is proportional to β and the sum of the characteristic convective-diffusive scalelengths (K_{zz}/V) upstream and downstream of the shock. Therefore τ_a is larger for weak shocks and for large values of K_{zz}, since particles diffuse to greater distances from the shock between shock encounters.

The two modifications introduce important new features. Equation (7) describes the escaping particles. Since $K_{zz}(p, z)$ is generally an increasing function of p, $\zeta_\infty(p)$ is generally a decreasing function of p so that the p-spectrum of the escaping particles is "harder" than that at the shock. This hardening occurs gradually as ζ increases, even in the case of no particle escape. Equation (6) shows that the escape of particles introduces an exponential rollover. Since the p-dependence of the rollover is determined by the p-dependence of $K_{zz}(p, z)$, which may be written as a product of v and a function of rigidity, the form of the rollover also depends on (Q/M) for each particle species (the general form of K_{zz} is presented in Sect. 3.4). Equations (5) and (6) also show the effect of an advected distribution $f_\infty(p)$ with a broad momentum spectrum. Equation (5) describes the spatial dependence upstream of the shock as $f(p)$ transitions from $f_0(p)$ at the shock to $f_\infty(p)$ far upstream. Equation (6) describes the modification of the accelerated particle spectrum at the shock by the form of $f_\infty(p)$. For example, if $f_\infty(p) = Cp^{-\gamma}S(p - p_0)$, where $S(x)$ is the Heaviside step function, and we neglect particle escape by taking $\zeta_\infty(p) \to \infty$, then we obtain

$$f_0(p) = \frac{\beta}{\beta-\gamma}Cp_0^{-\gamma}\left[\left(\frac{p}{p_0}\right)^{-\gamma}-\left(\frac{p}{p_0}\right)^{-\beta}\right]. \tag{12}$$

If $\beta < \gamma$ then at high energies $p \gg p_0$ the momentum power-law index is $-\beta$, as we obtained in Eq. (9) for particle injection out of the upstream plasma. However, if $\beta > \gamma$ then the momentum power-law index at high energies is $-\gamma$ and the shock effectively "lifts" the advected distribution while preserving the spectral index.

3.3 Shocks Modified by the Energetic Particles

Two further features of stationary planar DSA are worth noting even though they are not explicitly highlighted in Eqs. (5)–(7). The first is that if the pressure P of the accelerated particles is comparable with the thermal pressure of the plasma, then the energetic particles modify the plasma flow, which in turn modifies the particle acceleration. Neglecting magnetic fields and the MHD fluctuations in Eq. (2), the nonlinear modified shock structure

may be illustrated by taking the pressure moment of Eq. (2) for the same planar stationary configuration that we used in deriving Eqs. (4)–(8)

$$V_z \frac{dP}{dz} - \frac{d}{dz}\left(\overline{K_{zz}} \frac{dP}{dz}\right) + \gamma_e \frac{dV_z}{dz} P \simeq 0, \tag{13}$$

where $P = (4\pi/3)\int dp v p^3 f(p)$, γ_e is an effective ratio of specific heats varying between 5/3 for a non-relativistic distribution and 4/3 for a relativistic distribution, and $\overline{K_{zz}}$ is an effective diffusion coefficient independent of p, which weights $K_{zz}(p)$ according to the p-dependence of the diffusive flux. Equation (13) must then be augmented by the fluid equations describing the coupled evolution of the thermal plasma

$$\frac{d}{dz}(\rho V_z) = 0, \tag{14}$$

$$\rho V_z \frac{dV_z}{dz} = -\frac{d}{dz}(P_g + P), \tag{15}$$

$$V_z \frac{dP_g}{dz} + \gamma_g \frac{dV_z}{dz} P_g = 0, \tag{16}$$

where $\rho(z)$ is mass density, $P_g(z)$ is the pressure of the thermal gas, and $\gamma_g \simeq 5/3$ is the ratio of specific heats for the thermal gas. For the simple case of constant $\overline{K_{zz}}$, $\gamma_e = 5/3$, $P_g = 0$, $V_z(z \to \infty) = -V_0$ and $\rho(z \to \infty) = \rho_0$, we obtain

$$P(z) = \rho_0 V_0^2 \frac{2}{(\gamma_e + 1)} \frac{\exp(-V_0 z/\overline{K_{zz}})}{[1 + \exp(-V_0 z/\overline{K_{zz}})]}. \tag{17}$$

Equation (17) illustrates the growth of $P(z)$ through the shock from zero to, for this case of infinite Mach number, the value required for a strong shock. The pressure gradient decelerates the flow to the downstream density and velocity required by the Rankine-Hugoniot relations. In fact, shock modification is generally a small effect in the heliosphere; for example, the deceleration of the solar wind upstream of Earth's bow shock due to the accelerated proton pressure is ~5 %. Nevertheless shock modification may be more important in large SEP/ESP events in which a previous shock provides a population of advected energetic particles that are reaccelerated by the following shock wave as described in Sect. 2.5 (Eichler 1981; Gopalswamy et al. 2002). There is also evidence that the solar wind termination shock is modified by the low-energy ACRs (Florinski et al. 2009).

3.4 Wave Excitation by the Energetic Particles

The second noteworthy feature of DSA is the excitation of MHD turbulence by the accelerating ions, which we preface with a discussion of $\mathbf{K}(p)$. The spatial diffusion tensor contains all the complicated microphysics of the interactions of the charged particles with the fluctuating MHD fields of the plasma. Assuming axisymmetry of the fluctuating fields about the average magnetic field $\mathbf{B}$, the spatial diffusion tensor may be written as

$$K_{ij} = K_\perp \delta_{ij} + (K_\parallel - K_\perp) B_i B_j B^{-2}, \tag{18}$$

where $K_\parallel$ and $K_\perp$ are the diffusion coefficients parallel and perpendicular to $\mathbf{B}$, respectively. Since diffusive transport along $\mathbf{B}$ is generally more rapid than transport across $\mathbf{B}$, the diffusion coefficients generally satisfy $K_\parallel \gg K_\perp$. Quasilinear theory provides an expression for

$K_\parallel$ assuming a spectrum of Alfven waves propagating parallel to **B** as (Lee 1983; Gordon et al. 1999)

$$K_\parallel = \frac{v^2}{8}\int_{-1}^{1} d\mu \frac{1-\mu^2}{D_\mu} \tag{19}$$

with the particle pitch-angle diffusion coefficient given by

$$D_\mu = \frac{\pi}{2}\frac{\Omega^2}{B^2}\frac{1}{|\mu|v} I\left(k = \frac{\Omega}{\mu v}\right), \tag{20}$$

where $\Omega\,[= QB/(\Gamma Mc)]$ is the particle gyrofrequency, Γ is the particle Lorentz factor, μ is the cosine of the particle pitch angle, and $I(k)$ is the wave intensity as a function of wavenumber k, where

$$\left\langle |\delta \mathbf{B}|^2 \right\rangle = \int_{-\infty}^{\infty} dk I(k). \tag{21}$$

In Eq. (20) it is assumed that particle speeds are much larger than wave phase speeds. The fact that the wavenumber most important for scattering a particle is given by $k = \Omega/(\mu v)$ in Eq. (20) is due to the cyclotron resonance required for effective scattering of a charged particle by small-amplitude waves. It is clear from Eqs. (19) and (20) that the p- and (Q/M)-dependences of $K_\parallel$ through $I(k, z)$ determine the form and rigidity dependence of the exponential rollover in Eq. (6), the form and rigidity dependence of the escaping flux [Eq. (7)], and the rigidity dependence and energy spectrum of the energetic particle foreshock [Eq. (5)] (Tylka et al. 1999; Ng et al. 1999). Although $I(k)$ is due in part to fluctuations in the solar wind arising from the turbulent evolution of waves generated low in the corona, at the strongest shocks fluctuations upstream of the shock are enhanced at frequencies resonant with the accelerated particles due to a streaming instability driven by the accelerating protons. The instability is due to the pitch-angle anisotropy of the proton distribution function in the upstream plasma frame arising from diffusion due to the proton gradient; when these protons scatter on fluctuations propagating away from the shock in the plasma frame, they transfer a fraction $\sim V_A/v$ of their energy density to the fluctuations, where V_A is the Alfven speed. The enhanced wave intensity reduces $K_\parallel$, which reduces the spatial scale of the energetic particle foreshock, decreases the acceleration timescale [Eq. (11)], and increases the energy of the exponential rollover. Integrating the quasilinear wave kinetic equation and assuming that the unstable waves dominate $I(k, z)$ (Gordon et al. 1999), we obtain an implicit equation for $I(k, z)$ as

$$I(k,z) = I^0(k,z) + \frac{4\pi^2 V_A}{k^2 V}|Q_p| M_p \cos\psi \int_{|QB/ck|}^{\infty} dp v p^2 \left(1 - \frac{Q^2B^2}{c^2k^2p^2}\right)\left[f_p(p,z) - f_{p,\infty}(p)\right], \tag{22}$$

where the subscript p refers to protons, $I^0(k, z)$ is the ambient intensity of waves propagating in the unstable direction and $\cos\psi = |B_z/B|$. Wave enhancements as described in the small-amplitude limit by Eq. (22) are observed at most strong shocks (e.g. Hoppe et al. 1981; Tsurutani et al. 1983) unless the shocks are quasi-perpendicular, in which case the lower-energy protons that potentially dominate the energetic particle energy density in the plasma frame cannot participate in DSA (as will be described in Sect. 4.3). Although these waves

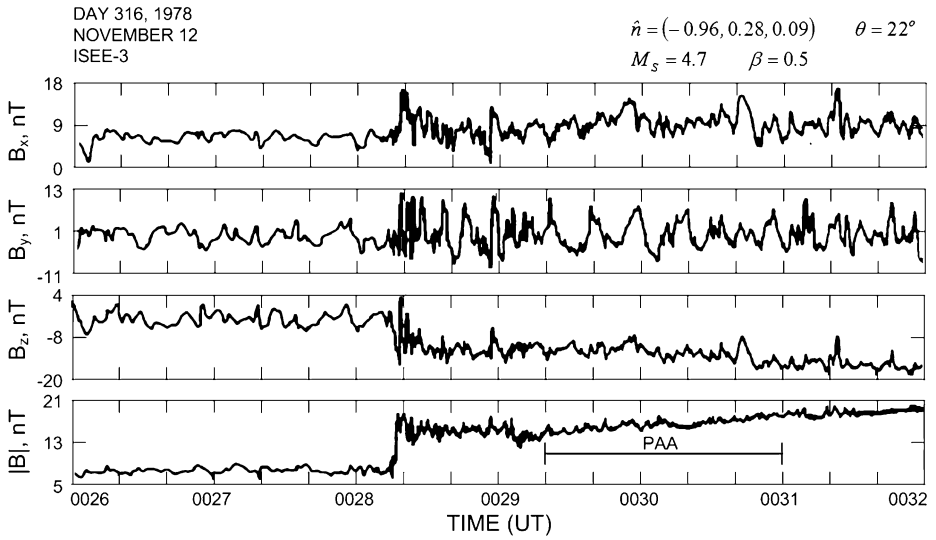

Fig. 16 Magnetic field components and magnitude for six minutes during passage of the interplanetary traveling shock of 12 November 1978 (adapted from Fig. 7 of Tsurutani et al. 1983). The large-amplitude variations both upstream and downstream of the shock are evident

are excited upstream, they are compressed and further enhanced at the shock and appear downstream as well. An example of these enhanced fluctuations at the shock event of 11, 12 November 1978 is shown in Fig. 16. The upstream waves observed at 1 AU typically have periods >20 s, extend ahead of and behind the shock by up to $\sim$1 hour, and have amplitudes of up to the ambient field strength.

3.5 Stochastic Acceleration

The last term on the LHS of Eq. (2) describes the process known as second-order Fermi acceleration, or more generally, stochastic acceleration. As it appears in Eq. (2) it describes the random walk of particles in **p**-space as they sample a stochastic sequence of electric field vectors $\delta\mathbf{E}$ due to MHD fluctuations (e.g. Lee and Völk 1975; Bogdan et al. 1991). The diffusion in **p**-space requires a broad spectrum of fluctuations and is dramatically enhanced if the particles and waves are in resonance. A stochastic acceleration term identical in form is also recovered from the first four terms on the LHS of Eq. (2) if it is assumed that **V** fluctuates (Jokipii and Lee 2010). In this case the process describes the random walk of particles in **p**-space due to the spatial random walk of particles through regions of compression and expansion where the particles are accelerated and decelerated, respectively. The velocity diffusion equation results from the spatial random walk of the particles in the presence of either a coherent variation of $\mathbf{V}(\mathbf{x}, t)$ (Ptuskin 1988; Zhang and Lee 2011) or a stochastic sequence of $\delta\mathbf{V}(\mathbf{x}, t)$ (Jokipii and Lee 2010). Although the stochastic diffusion coefficient D depends on the type of fluctuations contributing to $\delta\mathbf{E}$, this process generally suffers from small values of $D \propto [M\omega/(kp)]^2 \ll 1$ and limited energy density in the fluctuations. An exception may be the stochastic acceleration of SEPs in an impulsive solar flare event in the lower corona where the Alfven speed can be large so that D may be substantial. For the other energetic particle populations described in Sect. 1 shock acceleration is the more promising acceleration mechanism.

4 Complexity of Shocks and Their Associated Particles in Space

The standard analysis of DSA at a stationary planar shock is deceptively simple. It leaves the false impression that shock-associated energetic particle events can be reproduced by that model. The first complex aspect of virtually all shocks and their associated particles in the heliosphere is their spatial and temporal variation. Bow shocks at planetary magnetospheres or CMEs have varying magnetic obliquity and compression ratio, as well as a limited particle acceleration time within a given magnetic flux tube. The asymmetry of the solar wind termination shock between its nose and tail also leads to varying magnetic obliquity and compression ratio (McComas and Schwadron 2006). The large spatial scale of interplanetary shocks might suggest that they are planar and stationary except for the highest energy particles that sample the shock over large spatial and temporal scales, over which the shock parameters may vary systematically. However, local variations in solar wind parameters lead to warps in the shock front on the scale of the turbulent correlation length in the solar wind. The warps cause variations in magnetic obliquity and particle intensity along the shock front (Neugebauer and Giacalone 2005), and downstream turbulence due to variations in the resulting velocity downstream of the shock (Giacalone and Jokipii 2007). Figure 17 shows a simulation by Giacalone and Neugebauer (2008) of an interplanetary shock with no systematic variation of shock parameters along the shock front but propagating through density variations in the solar wind. The shock profiles at two different locations along the shock front separated by ∼8 correlation lengths are quite different. However, the energetic particle spectra at the two locations are similar since the particles average over variable conditions along the shock surface.

In addition, at interplanetary shocks adiabatic deceleration due to the expansion of the solar wind can compete with DSA and may also produce an exponential rollover in the particle energy spectra (Fisk and Lee 1980; Reames et al. 1997c).

4.1 The Dependence of the Power-Law Index $-\beta$ on Compression Ratio

The power-law index $-\beta$ of the particle spectrum at a planar stationary configuration with $\beta = 3X(X-1)^{-1}$ is a signature of DSA. However, most particle enhancements at a shock do not have the predicted index, even at energies below the exponential rollover expected from particle losses by escape, particle adiabatic deceleration, or limited shock lifetime. Figure 18 shows results from the study of van Nes et al. (1984) based on ISEE-3 data comparing the observed compression ratio X for 50 events with the observed energy power-law index $-\overline{\beta}$ of the particle differential intensity just downstream of the shock, where $\overline{\beta} = (\beta/2) - 1$. The data points would lie on the solid curve if $\overline{\beta} = (X+2)/(2X-2)$ as expected based on Eq. (9). The dashed curves allow for a ±25 % error in determining the compression ratios. Clearly the events do not exhibit the power law expected from DSA for ion injection at low energies even with a reasonable error in the measurement of X. However, the events in Category D, which show little change in the spectral index across the shock and tend to be accelerated by weak shocks, are apparently events in which an upstream distribution of energetic particles is "lifted" at the shock while retaining its spectral index as described by Eq. (12) with $\gamma < \beta$. These events are not expected to have the spectral index $\overline{\beta} = (X+2)/(2X-2)$ and are not expected to lie on the solid line. The events in Category C are so-called "shock spike" events (Sarris and Van Allen 1974) which peak at nearly perpendicular shocks and are thought to arise from scatter-free particle reflection at the increased strength of the magnetic field at a fast shock (Hudson 1965; Decker 1981). This process cannot be described by DSA; the spectrum is presumably determined by the advected upstream spectrum and should not satisfy $\overline{\beta} = (X+2)/(2X-2)$. The

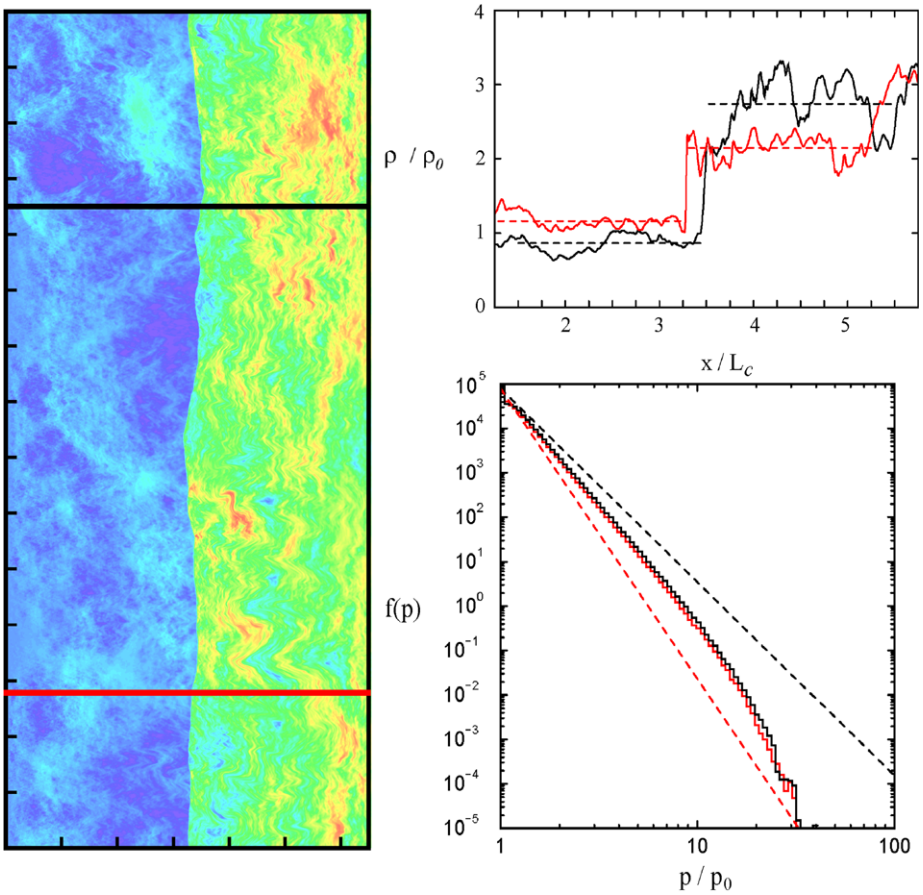

Fig. 17 (*Left*) An MHD/energetic-particle simulation of a shock moving through turbulence from right to left. The plasma density is indicated on a color scale from *dark blue* (*low*) to *red* (*high*). The density profile is shown along the *black* and *red lines* in the *upper right panel*. The energetic particle spectra are also shown for the *black* and *red cuts* in the *lower right panel* (from Giacalone and Neugebauer 2008)

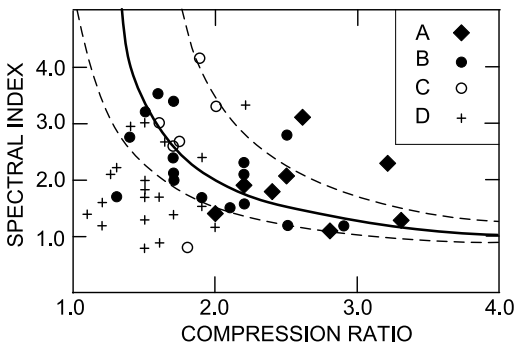

Fig. 18 Adapted from Fig. 12 of van Nes et al. (1984) showing the shock compression ratio X and the energy spectral index $\bar{\beta}$ for 50 ESP events in their sample for which X is available. The *solid curve* is the function $\bar{\beta}(X)$ expected based on Eq. (9); the dashed curves arise from ± 25 % uncertainty in X. The symbols, defined in the text, denote the four different classes of events

events in Category B are quasi-perpendicular shocks with irregular energetic particle profiles. These events may also exhibit scatter-free particle behavior since few particles have sufficient energy to achieve the mobility at the shock required for DSA and these particles are not sufficient to excite wave enhancements. The events of Category A are accelerated by oblique shocks and appear to have time profiles as expected from DSA. Nevertheless, even these events do not lie on the solid curve or even within the dashed curves. The resolution of this discrepancy may very well be that the scattering ions are actually scattered to isotropy in the average wave frame rather than the average plasma frame, where "average wave frame" refers to the average wave phase velocity of the resonant waves weighted by their intensities. What is therefore important is the average wave-frame compression ratio. The average wave frame downstream of the shock is determined by the transmission of the upstream waves; prediction of this quantity is complicated by the fact that the downstream wave spectrum includes all modes except those propagating shockwards in the shock frame. The upstream waves according to Eq. (22), however, are Alfven and magnetosonic waves propagating away from the shock in the plasma frame approximately parallel to the ambient magnetic field. Since the upstream wave enhancement has a phase velocity component parallel to the shock normal given by $V_{ph,z} = V_A \cos\psi$, we expect that the wave-frame compression ratio is smaller than X. This should shift the solid and dashed curves in Fig. 18 upwards by a fraction of order $V_{ph,z}/V$, although a quantitative prediction of the shift requires the difficult calculation of the downstream average wave frame. For interplanetary shocks, which are relatively weak at Earth orbit, $V_{ph,z}/V$ could be 10–20 %. Such a shift appears to move most of the Category A events closer to the solid curve. In an extensive study of the ESP event associated with the shock shown in Fig. 16, Kennel et al. (1986) noted that the observed power-law index is consistent with the predicted value based on the wave-frame compression ratio assuming that the plasma and wave frames are the same downstream and that the upstream waves are field-aligned Alfven waves. The remaining variations in Fig. 18 are very likely due to variation of the shock parameters along the shock as shown in Fig. 17; the compression ratio is determined locally, whereas the energetic particles have sampled the shock over a substantial fraction of its spatial extent and lifetime. Recent but similar studies by Lario et al. (2003) and Desai et al. (2004) based on ACE data find similar results. Even at lower energies of ~50 keV about a third of the shock events recorded in Lario et al. (2003) have no associated energetic particles. However, these events may be difficult to distinguish from the Category D events in the van Nes et al. (1984) study; at weak shocks with small injection rates out of the solar wind (as expected at nearly perpendicular shocks), the transition to the "lifted" spectrum at the shock may be difficult to detect.

4.2 Mechanisms of Ion Escape Upstream of the Shock

Although Eqs. (5)–(7) describe the loss of ions upstream of the shock by invoking a rapidly increasing spatial diffusion coefficient with increasing z, the actual cause of the ion loss and the exponential rollover of the distribution function is more complex. The time dependence of shock acceleration can lead to the evolution of the foreshock ion distribution and energy spectrum toward the form given by Eqs. (5) and (6) for $\zeta_\infty \to \infty$. Since interplanetary travelling shocks tend to weaken with time, a more likely possibility is that the proton-excited wave enhancement decays with increasing heliocentric radial distance so that K_{zz} increases with time. In addition, the escape of ions is enhanced by anti-sunward magnetic mirroring in the field upstream of the shock (Lee 2005). This process is included in the focused transport equation (e.g. Roelof 1969; Earl 1976; Isenberg 1997). A similar effect is also obtained in solutions of the telegrapher's equation (modeling the diffusive escape of

particles which have a finite speed), which show that some particles are able to race ahead of the diffusive wake (Morse and Feshbach 1953). Planetary bow shocks are sufficiently small that drift transport across field lines, or advection of a given flux tube along the shock surface, can transport the accelerating particles to a weaker portion of the shock where acceleration is slower or ions may escape upstream through the weaker turbulence. The advection of flux tubes along the shock surface is also thought to play an important role at the solar wind termination shock where the ACRs are primarily accelerated on the flanks and towards the heliospheric tail rather than near the nose (McComas and Schwadron 2006; Schwadron et al. 2008; Kota 2008).

The upstream escape of particles at shocks in the solar wind is important in order to account for the observed temporal structure of SEP events. The escaping particles are first to arrive at Earth orbit, they forecast the arrival of higher SEP intensities at later times, and, since they were accelerated closer to the Sun where acceleration rates are higher, they usually contain the highest energy particles. As is evident in Eq. (11), the acceleration rate is inversely proportional to the spatial diffusion coefficient. Since the scattering mean free path generally scales with a power of the particle gyroradius, the acceleration rate is controlled by the gyrofrequency Ω, which is proportional to B. Within the orbit of Earth $B \propto r^{-2}$, which is much larger close to the Sun. In the model described by Eqs. (4)–(7) the escaping particle flux is given by expression (7). According to Eqs. (19) and (20), if $I \propto k^{-\alpha}$, then $K_{zz} \propto v(p/Q)^{2-\alpha}$, which implies the scattering mean free path $\lambda \propto (p/Q)^{2-\alpha}$. Since the parameter α is generally observed to lie in the range $1 < \alpha < 2$, K_{zz} generally increases with increasing p. Therefore, the denominator on the RHS of Eq. (7) becomes ζ_∞ at high energies and the escaping flux is harder than the intensity at the shock. An interesting consequence of the dominance of proton-excited waves in the foreshock is evident in Eq. (22). Since $\zeta_\infty \sim f_0 - f_\infty$, the escaping flux at high energies is approximately independent of the accelerating particle intensity as long as it is large enough to produce wave intensities larger than that in the ambient solar wind. This feature greatly reduces the variability of the escaping flux and leads to the "streaming limit" of the escaping proton intensity identified and interpreted by Reames and colleagues (Reames 1990; Ng and Reames 1994; Reames and Ng 1998, 2010).

4.3 Ion Injection at the Shock Front

Perhaps the most complex and controversial issue within the theory of shock acceleration is the rate at which thermal plasma is injected at the shock front into the process of DSA. Equation (2) formally requires near isotropy of the particle distribution function. This condition is clearly not satisfied in the frame of the shock for the bulk of the upstream thermal plasma, which impinges on the shock front with Mach number greater than unity. Even though Eq. (2) is not satisfied, a small fraction of the incident ions is reflected at the shock front, drifts parallel to the motional electric field given by the first term on the RHS of Eq. (1), and is sufficiently mobile and energetic to propagate back upstream. These ions have begun the process of first-order Fermi/shock acceleration even though they may not formally satisfy near isotropy and $v \gg V$ as required for the validity of Eq. (2). This injection process has been observed in detail at Earth's bow shock as a solar wind flux tube is swept into the bow shock. When the angle between the upstream magnetic field and the shock normal, ψ, is reduced to $\psi \approx 65°$–$70°$ (Paschmann et al. 1981; Bonifazi and Moreno 1981), field-aligned beams of protons begin to stream along the upstream magnetic field away from the bow shock with energies of a few keV/nucleon. A similar process presumably occurs at interplanetary shocks although their nearly stationary structure with turbulent upstream conditions adjacent to the shock must produce a more diffuse injection at the shock front.

It is evident from this discussion that the magnetic obliquity of a shock is critical for injection of thermal plasma. This issue is complicated by the meandering of magnetic field lines on scales much larger than the energetic particle gyroradii so that the shock obliquity varies not only in response to shock warps but also due to field line meandering. This variation contributes to the spatial and temporal variation of the energetic particle intensity along the shock front as injection rates and acceleration rates vary [see Eqs. (11) and (18)] since K_{zz} depends on obliquity. The meandering also contributes in general to $K_\perp$, which describes spatial diffusion perpendicular to the average magnetic field (Jokipii 1971).

An interesting question is whether there is an effective energy threshold for injection as a function of ψ. A reasonable answer is "yes" since a particle can only access the upstream plasma if $v > V\sec\psi$, unless transport normal to the average field is effective, as would be expected if there is significant field-line meandering. It is important to note that such a particle may have originated in the upstream thermal distribution and subsequently accelerated at the shock front to exceed the threshold. Thus, this threshold does not provide an injection rate since it is unclear what fraction of the incident thermal distribution attains the threshold. In any case, if this condition is satisfied for an ion reflected upstream, then the first-order Fermi acceleration process is underway.

An informative exercise is to calculate the anisotropy magnitude of the distribution function resulting for stationary planar DSA as described by Eqs. (8) and (9) with constant K_{zz}. The anisotropy magnitude in the shock frame is (Giacalone and Jokipii 1999)

$$|\mathbf{A}| = 3\frac{|\mathbf{S}|}{vf} = 3\frac{V}{v}\left[\left(\frac{\beta}{3}-1\right)^2 + \frac{K_A^2\sin^2\psi + (K_\parallel - K_\perp)^2\sin^2\psi\cos^2\psi}{(K_\parallel\cos^2\psi + K_\perp\sin^2\psi)^2}\right]^{1/2}, \quad (23)$$

where $K_A = v^2/(3\Omega)$. The streaming $\mathbf{S}$, which is the differential (in p) flux density in phase space averaged over momentum directions, is given by

$$\mathbf{S} = -\mathbf{K}\cdot\nabla f - (1/3)\mathbf{V}(p\partial f/\partial p) + (pvc)\left(3QB^2\right)^{-1}\mathbf{B}\times\nabla f. \quad (24)$$

A reasonable condition that the Parker equation is satisfied and that particles are sufficiently mobile to participate in DSA is $|\mathbf{A}| \ll 1$. If we define the threshold speed v_{th} for DSA to occur by $|\mathbf{A}| = 1$ and if $K_\parallel \gg K_\perp, K_A$, then according to Eq. (23)

$$v_{th} = 3V\left[\left(\frac{\beta}{3}-1\right)^2 + \tan^2\psi\right]^{1/2}, \quad (25)$$

which is similar in form to the intuitive threshold mentioned above [for $\beta = 6$ Eq. (25) is proportional to that intuitive expression while ensuring that a substantial fraction of the nearly isotropic distribution can propagate upstream]. The anisotropy in the z-direction of a spherical coordinate system is generally defined in terms of the phase space distribution function $F(p,\mu)$ as $A(p) = [F(p,1) - F(p,-1)]/[F(p,1) + F(p,1)]$. Assuming a linear dependence of $F(p,\mu)$ on μ, we obtain in general $\mathbf{A}(p) = 3\mathbf{S}/(vf)$, which is expressed in Eq. (23).

Equation (23) yields a different behavior for $v_{th}(\psi)$ as $\psi \to \pi/2$. The function $v_{th}(\psi)$ peaks and then decreases to a locally minimum value at $\psi = \pi/2$ (Zank et al. 2006) given by

$$v_{th} = 3V\left[\left(\frac{\beta}{3}-1\right)^2 + \left(\frac{K_A}{K_\perp}\right)^2\right]^{1/2}. \quad (26)$$

For the case of "hard sphere" scattering (Jokipii 1987) we have

$$K_\perp / K_\parallel = \left(1+\eta^2\right)^{-1}, \tag{27}$$

where $\eta = \lambda_\parallel / r_g$, $\lambda_\parallel$ is the scattering mean free path parallel to $\mathbf{B}$, and $r_g\,(= v/\Omega)$ is approximately the particle gyroradius. In this case Eq. (26) becomes

$$v_{th} = 3V\left[\left(\frac{\beta}{3}-1\right)^2 + \left(\frac{1+\eta^2}{\eta}\right)^2\right]^{1/2}. \tag{28}$$

Unless the upstream magnetic field is highly turbulent we have $\eta \gg 1$. Therefore, $v_{th} \simeq 3V\eta \gg V$, indicating a large energy threshold. The condition $v_{th} \simeq V\eta$ is the requirement for diffusive shock acceleration at a perpendicular shock given by Jokipii (1987) based on three separate arguments including the requirement of small anisotropy. The origin of the anisotropy that limits DSA to speeds $v > v_{th}$ is different for quasi-parallel shocks [Eq. (25)] and quasi-perpendicular shocks [Eq. (26)]. The former is due to diffusive streaming along the upstream magnetic field and the latter is due to drift streaming along the shock front. The speed threshold is clearly far more restrictive for quasi-perpendicular shocks. As emphasized above, this discussion does not address what fraction of the incident thermal plasma is injected into DSA at the shock front by a process that is not diffusive and may involve large anisotropies. Field-aligned beams at Earth's quasi-perpendicular bow shock are produced by mirroring (reflection) and drift at the shock front but they cannot propagate upstream to initiate DSA unless Eq. (25) is satisfied. Nevertheless, observations seem to support a lower injection rate at nearly perpendicular shocks (van Nes et al. 1984).

However, we emphasize that field-line meandering can strongly enhance cross-field transport of low-energy ions (e.g. Giacalone and Jokipii 1999). In fact, it can be shown that for very low-energy ions moving within magnetic turbulence that is typical of that in the solar wind, the perpendicular diffusion coefficient $K_\perp$ can exceed K_A. In this case, the injection threshold at a perpendicular shock is only slightly larger than that at a parallel shock. In fact, self-consistent hybrid simulations have shown that even thermal plasma can be accelerated by a perpendicular shock moving through a plasma containing pre-existing large-scale magnetic fluctuations (Giacalone 2005).

In spite of the uncertainty in the physics of the injection process, Eq. (11), together with Eq. (18) and $K_\parallel \gg K_\perp$, show that the acceleration timescale at nearly perpendicular shocks is much shorter than that at a parallel shock (Jokipii 1987). If a particular shock event has quasi-parallel and quasi-perpendicular phases along the observer's magnetic field line, then particles accelerated in the quasi-parallel phase should have higher intensity (due to higher injection rates out of the solar wind plasma) and lower energy (due to smaller acceleration rates). Similarly, the particles accelerated in the quasi-perpendicular phase should have lower intensity (due to lower injection rates of solar wind plasma, but straightforward injection of remnant suprathermal or energetic particles) and higher energy (due to higher acceleration rates). Since the solar wind and remnant energetic ions have markedly different composition (e.g. Mason et al. 1999a; Desai et al. 2006b; Mewaldt et al. 2007; the remnant particles contain higher fractions of heavy ions, notably Fe, and ^{3}He), one expects compositional fractionation between high and low energies. Tylka and Lee (2006) have found that the fluence ratio Fe/O as a function of energy supports this scenario. Papers that emphasize the importance of SEP contributions from the concomitant flare include Cane et al. (2003, 2006), and Masson et al. (2009). This issue is also discussed in Mewaldt et al. (2007) and Tylka et al. (2005). Clearly the energetic particles observed by

a particular observer in a specific event arise from a superposition of sources and transport trajectories, each of which experienced acceleration at a sequence of varying shock configurations in space and time. Attempting to infer the source distribution, and the temporal and spatial evolution of the shock, from the measured energetic particle time profiles at one (or even two or three locations) is a challenge indeed.

4.4 Ion Shock Acceleration Close to the Sun

A common criticism of the shock origin of gradual events is the prompt arrival of ~100 MeV/nucleon ions in some events, implying escape from the shock when the CME is only ~4 R_s (solar radii) from the Sun. When combined with the time required to form the shock wave, accounting for such acceleration efficiency is indeed a challenge. However, it must be recognized that $B \propto r^{-2}$ within the inner heliosphere. Since $\lambda_{\parallel} \propto r_g \propto r^2$, the timescale for acceleration τ_a satisfies $\tau_a \propto r^2$, implying extremely efficient acceleration close to the Sun. In addition, although the CME-driven shock can be as rapid as 2000–3000 km/s, the Mach number, and therefore also the compression ratio, may not be large and in any case is difficult to determine. The Alfven speed dominates the MHD fast speed in the corona and depends on the complex magnetic field structure at the flaring active region. One popular radial profile of the Alfven speed is presented by Mann et al. (2003), which increases from ~400 km/s to ~700 km/s between 1.5 and 4 R_s from Sun center, and then gradually decreases as $V_A \propto r^{-1}$ out to ~20 R_s before approaching a constant value at large heliocentric radial distances. Although the Mach number and compression ratio are not large at the peak of the Alfven speed, acceleration to high energy could be efficient at either $r < 4$ R_s if the shock has formed in this low region of the corona, or in the range $r > 4$ R_s before the CME has begun to decelerate. Clearly a detailed model of the shock driven by the CME is required for a quantitative assessment of particle acceleration near the Sun. Nevertheless shock acceleration close to the Sun appears to be the most promising acceleration mechanism for the SEP phase of gradual events. It will be very exciting to observe SEP events with Solar Orbiter and Solar Probe close to the Sun.

4.5 Long-Time Behavior of SEPs

Another interesting feature of SEP events is their long-time behavior. Multi-spacecraft studies have shown that large events spread nearly uniformly throughout the inner heliosphere in their decay phase with "invariant" power-law energy spectra for all ion species (Reames et al. 1997a, 1997b). The events decay, presumably by adiabatic deceleration and slow escape to large heliocentric radial distances. The escape rate is presumably reduced by the Archimedes spiral magnetic field, which creates a confining "reservoir" in the inner heliosphere. As these events extend in volume they may coalesce with other events to form "super events" (McKibben 1972). Some coalesced events may still be modified by a large shock remaining from a coalescence of individual shock events (Pyle et al. 1984). In other events the shocks decay while their accelerated particles escape the decaying turbulence adjacent to the shock and fill the inner heliosphere. To our knowledge a detailed theoretical description of events transitioning to, or in, the decay phase does not exist. During solar maximum conditions these events may ensure a supply of remnant energetic particles for reacceleration at new shock waves.

4.6 Upstream Nonlinear Waves

Finally, we emphasize that shocks, including particle acceleration as one important channel of dissipation, are nonlinear structures involving coupled large-amplitude changes in the particle parameters and electromagnetic fields. Although the simplest versions of DSA describe the energetic particles using Eq. (2) as a linear equation in which the coefficients are independent of the energetic particle distribution, Eqs. (13)–(16) show that the energetic particles may influence the plasma bulk flow and Eq. (22) shows that the energetic particles excite waves that modify the diffusion coefficients. Other nonlinearities occur when the excited waves grow to large amplitude. Nonlinear wave-wave interactions can modify the excited wave intensity, and therefore the spatial diffusion coefficient. Upstream of Earth's bow shock the compressive large-amplitude magnetosonic waves are observed to steepen into "shocklets" with whistler precursors (Hoppe et al. 1981; Hada et al. 1987). Even more dramatic are the Short Large-Amplitude Magnetic Structures (SLAMS) observed at Earth's bow shock (Schwartz and Burgess 1991; Lucek et al. 2008) that grow to magnetic field magnitudes several times that of the ambient field, presumably due to their effective reflection of the accelerating ions and the effective transfer of energy from the ions to the waves. A related phenomenon that may occur at a very strong shock with a turbulent foreshock was predicted by Bell and Lucek (2001) and further developed by Bell (2004) (see also Schure et al. 2012, this issue): The foreshock turbulence and the discrepancy between the energetic ion and plasma electron gyroradii hinder the cancellation of the energetic ion and plasma currents. This results in a Lorentz force on the bulk plasma and a nonresonant instability that in turn leads to an enhancement of the average foreshock magnetic field strength. The increased field strength reduces the spatial diffusion coefficient and the acceleration timescale [according to Eq. (11)] with important consequences for cosmic ray acceleration at supernova remnant shocks.

5 Conclusions

With a variety of sites and plasma configurations, and measurements by many spacecraft in different locations, the heliosphere is an ideal space plasma environment in which to investigate particle acceleration. Based on these detailed observations, and the theories and understanding they generate, inferences may be drawn about the acceleration processes that operate at various sites throughout the Galaxy and beyond. In this review we have focused on SEP events and their acceleration at CME-driven coronal/interplanetary shock waves. Although the observed temporal/spatial behavior, energy spectra and composition of these events are broadly consistent with the theory of diffusive shock acceleration in its simplest form, there remain puzzles, discrepancies, and therefore challenges. The broad range of SEP intensities observed with similar CME speeds is one well-advertised puzzle. The lack of a theory of thermal plasma injection at the shock front as a function of shock strength and magnetic obliquity is another. The rate of ion escape upstream of the foreshock, which affects the form of the energy spectral rollover, is yet another, as is the nonlinear evolution and magnetic field amplification in the foreshock that dictates the acceleration timescale. Some of these puzzles hinge on our inadequate understanding of particle propagation in turbulent electromagnetic fields and the limitations of diffusive spatial transport. Others depend on the restrictions of the Parker transport Eq. (2) to high particle speeds and small anisotropy in velocity space. All of these issues require interesting modifications and extensions of the simplest theory guided by current and future detailed measurements. Solar Cycle 24 will provide new events and in 2017/2018 Solar Orbiter and Solar Probe Plus will provide a completely new view of SEP events close to the Sun.

Acknowledgements The authors wish to acknowledge the hospitality of the International Space Science Institute, the stimulating program of the Workshop on Particle Acceleration in Cosmic Plasmas, and the patience of Dr. Andre Balogh while awaiting this typescript. The contribution of M.A.L. was supported, in part, by NASA grants NNX08AJ13G, NNX11AO97G and NNX12AB32G. The contribution of R.A.M. was sponsored by NASA under grants NNX8AI11G, NNX06AC21G, and under subcontract SA2715-26309 from UC Berkeley under NASA contract NAS5-03131. The contribution of J.G. was supported, in part, by NASA grants NNX11AO64G and NNX10AF24G.

References

O. Adriani et al., Observations of the 2006 December 13 and 14 solar particle events in the 80 MeV^{n-1}-3 GeV^{n-1} range from space with the PAMELA detector. Astrophys. J. **742**, 102 (2011)

W.I. Axford, Acceleration of cosmic rays by shock waves, in *Proc. Int. Conf. Cosmic Rays 17th*, vol. 12 (1981), p. 155

W.I. Axford, E. Leer, G. Skadron, The acceleration of cosmic rays by shock waves, in *Proc. Int. Conf. Cosmic Rays 15th*, vol. 11, (1977), p. 132

D. Band et al., Batse observations of gamma ray burst spectra. 1—Spectral diversity. Astrophys. J. **413**, 281 (1993)

A.R. Bell, The acceleration of cosmic rays in shock fronts. Mon. Not. R. Astron. Soc. **182**, 147 (1978)

A.R. Bell, Turbulent amplification of magnetic field and diffusive shock acceleration of cosmic rays. Mon. Not. R. Astron. Soc. **353**, 550 (2004)

A.R. Bell, S.G. Lucek, Cosmic ray acceleration to very high energy through the non-linear amplification by cosmic rays of the seed magnetic field. Mon. Not. R. Astron. Soc. **321**, 433 (2001)

R.D. Blandford, J.P. Ostriker, Particle acceleration by astrophysical shocks. Astrophys. J. **221**, L29 (1978)

P. Bochsler, E. Möbius, Energetic neutral atoms: an additional source for heliospheric pickup ions. Astrophys. J. **721**, L6 (2010)

T.J. Bogdan, M.A. Lee, P. Schneider, Coupled quasi-linear wave damping and stochastic acceleration of pickup ions in the solar wind. J. Geophys. Res. **96**, 161 (1991)

C. Bonifazi, G. Moreno, Reflected and diffuse ions backstreaming from the Earth's bow shock, 2. Origin. J. Geophys. Res. **86**, 4405 (1981)

H.H. Breneman, E.C. Stone, Solar coronal and photospheric abundances from solar energetic particle measurements. Astrophys. J. **299**, L57 (1985)

D. Burgess, E. Möbius, M. Scholer, Ion acceleration at the Earth's bow shock. Space Sci. Rev. (2012, this issue). doi:10.1007/s11214-012-9901-5

M. Bzowski, M. Krolikowska, Are the sungrazing comets the inner source of pickup ions and energetic neutral atoms? Astron. Astrophys. **435**, 723 (2005)

H.V. Cane, T.T. von Rosenvinge, C.M.S. Cohen, R.A. Mewaldt, Two components in major solar particle events. Geophys. Res. Lett. **30**, 8017 (2003). doi:10.1029/2002GL016580

H.V. Cane, R.A. Mewaldt, C.M.S. Cohen, T.T. von Rosenvinge, Role of flares and shocks in determining solar energetic particle abundances. J. Geophys. Res. **111**, A06S90 (2006). doi:10.1029/2005JA011071

P.J. Cargill, L. Vlahos, G. Baumann, J.F. Drake, A. Nordlund, Current fragmentation and particle acceleration in solar flares. Space Sci. Rev. (2012, this issue). doi:10.1007/s11214-012-9888-y

S.V. Chalov, H.J. Fahr, Energetic particles from the outer heliosphere appearing as a secondary pick-up ion component. Astron. Astrophys. **401**, L1 (2003)

C.M.S. Cohen et al., New observations of heavy-ion-rich solar particle events from ACE. Geophys. Res. Lett. **26**, 2697 (1999a)

C.M.S. Cohen et al., Inferred charge states of high energy solar particles from the solar isotope spectrometer on ACE. Geophys. Res. Lett. **26**, 149 (1999b)

C.M.S. Cohen et al., Heavy ion abundances and spectra from the large solar energetic particle events of October-November 2003. J. Geophys. Res. **110**, A09S16 (2005). doi:10.1029/2005JA011004

R.B. Decker, The modulation of low-energy proton distributions by propagating interplanetary shock waves: a numerical simulation. J. Geophys. Res. **86**, 4537 (1981)

M.I. Desai et al., Spectral properties of heavy ions associated with the passage of interplanetary shocks at 1 AU. Astrophys. J. **611**, 1156 (2004)

M.I. Desai et al., Heavy-ion elemental abundances in large solar energetic particle events and their implications for the seed population. Astrophys. J. **649**, 470 (2006a)

M.I. Desai, G.M. Mason, J.E. Mazur, J.R. Dwyer, Solar cycle variations in the composition of the suprathermal heavy-ion population near 1 AU. Astrophys. J. **645**, L81 (2006b)

L.O'C. Drury, An introduction to the theory of diffusive shock acceleration of energetic particles in tenuous plasmas. Rep. Prog. Phys. **46**, 973 (1983)
L.O'C. Drury, W.I. Axford, D. Summers, Particle acceleration in modified shocks. Mon. Not. R. Astron. Soc. **198**, 833 (1982)
J.A. Earl, The effect of adiabatic focusing upon charged particle propagation in random magnetic fields. Astrophys. J. **205**, 900 (1976)
D. Eichler, A cosmic ray mediated shock in the solar system. Astrophys. J. **247**, 1089 (1981)
D.C. Ellison, R. Ramaty, Shock acceleration of electrons and ions in solar flares. Astrophys. J. **298**, 400 (1985)
A.G. Emslie et al., Energy partition in two solar flare/CME events. J. Geophys. Res. **109**, A10104 (2004). doi:10.1029/2004JA010571
A.G. Emslie, B.R. Dennis, G.D. Holman, H.S. Hudson, Refinements to flare energy estimates: a followup to "Energy partition in two solar flare/CME events" by A.G. Emslie et al. J. Geophys. Res. **110**, A11103 (2005). doi:10.1029/2005JA011305
A. Falcone et al., Observation of GeV solar energetic particles from the 1997 November 6 event using Milagrito. Astrophys. J. **588**, 557 (2003)
E. Fermi, On the origin of the cosmic radiation. Phys. Rev. **75**, 1169 (1949)
E. Fermi, Galactic magnetic fields and the origin of cosmic radiation. Astrophys. J. **119**, 1 (1954)
L.A. Fisk, G. Gloeckler, Acceleration of suprathermal tails in the solar wind. Astrophys. J. **686**, 1466 (2008)
L.A. Fisk, G. Gloeckler, Particle acceleration in the heliosphere: implications for astrophysics. Space Sci. Rev. (2012, this issue). doi:10.1007/s11214-012-9899-8
L.A. Fisk, M.A. Lee, Shock acceleration of energetic particles in corotating interaction regions in the solar wind. Astrophys. J. **237**, 620 (1980)
V. Florinski, R.B. Decker, J.A. le Roux, G.P. Zank, An energetic-particle-mediated termination shock observed by Voyager 2. Geophys. Res. Lett. **36**, L12101 (2009). doi:10.1029/2009GL038423
S.E. Forbush, Three unusual cosmic-ray increases possibly due to charged particles from the Sun. Phys. Rev. **70**, 771 (1946)
M.A. Forman, L.O'C. Drury, Time dependent shock acceleration: approximations and exact solutions, in *Proc. Int. Conf. Cosmic Rays 18th*, vol. 2 (1983), p. 267
J. Geiss, G. Gloeckler, L.A. Fisk, R. von Steiger, C+ pickup ions in the heliosphere and their origin. J. Geophys. Res. **100**, 23373 (1995)
J. Giacalone, The efficient acceleration of thermal protons by perpendicular shocks. Astrophys. J. **628**, L37 (2005)
J. Giacalone, J.R. Jokipii, The transport of cosmic rays across a turbulent magnetic field. Astrophys. J. **520**, 204 (1999)
J. Giacalone, J.R. Jokipii, Magnetic field amplification by shocks in turbulent fluids. Astrophys. J. **663**, L41 (2007)
J. Giacalone, J.R. Jokipii, Suprathermal ions associated with strong interplanetary shocks, in *Particle Acceleration and Transport*. AIP Conf. Proc., vol. 1436 (AIP, New York, 2012), p. 130
J. Giacalone, M. Neugebauer, The energy spectrum of energetic particles downstream of turbulent collisionless shocks. Astrophys. J. **673**, 629 (2008)
J. Giacalone, J.F. Drake, J.R. Jokipii, The acceleration mechanism of anomalous cosmic rays. Space Sci. Rev. (2012, this issue). doi:10.1007/s11214-012-9915-z
G. Gloeckler et al., Acceleration of interstellar pickup ions in the disturbed solar wind observed on Ulysses. J. Geophys. Res. **99**, 17637 (1994)
G. Gloeckler et al., Interception of comet Hyakutake's ion tail at a distance of 500 million kilometres. Nature **404**, 576 (2000a)
G. Gloeckler, L.A. Fisk, J. Geiss, N.A. Schwadron, T.H. Zurbuchen, Elemental composition of the inner source pickup ions. J. Geophys. Res. **105**, 7459 (2000b)
G. Gloeckler et al., Sources, injection and acceleration of heliospheric ion populations, in *Acceleration and Transport of Energetic Particles Observed the Heliosphere: ACE 2000 Symposium*, ed. by R.A. Mewaldt et al., AIP Conference Proceedings, vol. 528 (AIP, New York, 2000c), p. 221
N. Gopalswamy, Coronal mass ejections of Solar Cycle 23. J. Astrophys. Astron. **27**, 243 (2006)
N. Gopalswamy et al., Interacting coronal mass ejections and solar energetic particles. Astrophys. J. **572**, L103 (2002)
N. Gopalswamy, S. Yashiro, S. Krucker, G. Stenborg, R.A. Howard, Intensity variation of large solar energetic particle events associated with coronal mass ejections. J. Geophys. Res. **109**, A12105 (2004). doi:10.1029/2004JA010602
N. Gopalswamy, H. Xie, S. Yashiro, S. Akiyama, P. Mäkelä, I.G. Usoskin, Properties of ground level enhancement events and the associated solar eruptions during Solar Cycle 23. Space Sci. Rev. (2012). doi:10.1007/s11214-012-9890-4

B.E. Gordon, M.A. Lee, E. Möbius, K.J. Trattner, Coupled hydromagnetic wave excitation and ion acceleration at interplanetary traveling shocks and Earth's bow shock revisited. J. Geophys. Res. **104**, 28263 (1999)
T. Hada, C.F. Kennel, T. Terasawa, Excitation of compressional waves and the formation of shocklets in the Earth's foreshock. J. Geophys. Res. **92**, 4423 (1987)
E.A. Helder, J. Vink, A.M. Bykov, Y. Ohira, J.C. Raymond, R. Terrier, Observational signatures of particle acceleration in supernova remnants. Space Sci. Rev. (2012, this issue). doi:10.1007/s11214-012-9919-8
M.M. Hoppe, C.T. Russell, L.A. Frank, T.E. Eastman, E.W. Greenstadt, Upstream hydromagnetic waves and their association with backstreaming ion populations—ISEE 1 and 2 observations. J. Geophys. Res. **86**, 4471 (1981)
P.D. Hudson, Reflection of charged particles by plasma shocks. Mon. Not. R. Astron. Soc. **131**, 23 (1965)
P.A. Isenberg, A hemispherical model of anisotropic interstellar pickup ions. J. Geophys. Res. **102**, 4719 (1997)
J.R. Jokipii, Propagation of cosmic rays in the solar wind. Rev. Geophys. Space Phys. **9**, 27 (1971)
J.R. Jokipii, Rate of energy gain and maximum energy in diffusive shock acceleration. Astrophys. J. **313**, 842 (1987)
J.R. Jokipii, M.A. Lee, Compression acceleration in astrophysical plasmas and the production of $f(v) \propto v^{-5}$ spectra in the heliosphere. Astrophys. J. **713**, 475 (2010)
S.W. Kahler, The correlation between solar energetic particle peak intensities and speeds of coronal mass ejections: effects of ambient particle intensities and energy spectra. J. Geophys. Res. **106**, 20947 (2001)
S.W. Kahler et al., Associations between coronal mass ejections and solar energetic proton events. J. Geophys. Res. **89**, 9683 (1984)
C.F. Kennel, F.V. Coroniti, F.L. Scarf, W.A. Livesey, C.T. Russell, E.J. Smith, A test of Lee's quasi-linear theory of ion acceleration by interplanetary traveling shocks. J. Geophys. Res. **91**, 11917 (1986)
B. Klecker, E. Möbius, M.A. Popecki, Ionic charge states of solar energetic particles: a clue to the source. Space Sci. Rev. **130**, 273 (2007)
J. Kota, Anomalous cosmic rays at a blunt termination shock, in *Proc. Int. Conf. Cosmic Rays 30th*, vol. 1 (2008), p. 853
G.F. Krymsky, A regular mechanism for the acceleration of charged particles on the front of a shock wave. Dokl. Akad. Nauk SSSR **234**, 1306 (1977)
H. Kucharek et al., On the source and acceleration of energetic He^{+}: a long-term observation with ACE/SEPICA. J. Geophys. Res. **108**(A10), 8040 (2003). doi:10.1029/2003JA009938
J. Kunches (2005). http://umbra.nascom.nasa.gov/SEP/
D. Lario, G.C. Ho, R.B. Decker, E.C. Roelof, M.I. Desai, C.W. Smith, ACE observations of energetic particles associated with transient interplanetary shocks, in *Solar Wind Ten*. AIP Conference Proceedings, vol. 679 (AIP, New York, 2003) 640
M.A. Lee, Coupled hydromagnetic wave excitation and ion acceleration upstream of the Earth's bow shock. J. Geophys. Res. **87**, 5063 (1982)
M.A. Lee, Coupled hydromagnetic wave excitation and ion acceleration at interplanetary traveling shocks. J. Geophys. Res. **88**, 6109 (1983)
M.A. Lee, Coupled hydromagnetic wave excitation and ion acceleration at an evolving coronal/interplanetary shock. Astrophys. J. Suppl. **158**, 38 (2005)
M.A. Lee, H.J. Völk, Hydromagnetic waves and cosmic ray diffusion theory. Astrophys. J. **198**, 485 (1975)
R.A. Leske et al., Solar isotopic composition as determined using solar energetic particles. Space Sci. Rev. **130**, 195 (2007). doi:10.1007/s11214-007-9185-3
G. Li, G.P. Zank, Mixed particle acceleration at CME-driven shocks and flares. Geophys. Res. Lett. **32**, L02101 (2005a). doi:10.1029/2004GL021250
G. Li, G.P. Zank, Multiple CMEs and large gradual SEP events, in *Proc. Int. Conf. Cosmic Rays 29th*, vol. 1 (2005b), p. 173
G. Li, G.P. Zank, W.K.M. Rice, Acceleration and transport of heavy ions at coronal mass ejection-driven shocks. J. Geophys. Res. **110**, A06104 (2005). doi:10.1029/2004JA010600
G. Li et al., Shock geometry and spectral breaks in large SEP events. Astrophys. J. **702**, 998 (2009)
G. Li, R. Moore, R.A. Mewaldt, L. Zhao, A.W. Labrador, A twin-CME scenario for ground level enhancement events. Space Sci. Rev. (2012). doi:10.1007/s11214-011-9823-7
R.P. Lin, Energy release and particle acceleration in flares: summary and future prospects. Space Sci. Rev. **159**, 421 (2011). doi:10.1007/s11214-011-9801-0
C. Lopate, Fifty years of ground level solar particle event observations, in *Solar Eruptions and Energetic Particles*, ed. by N. Gopalswamy, R.A. Mewaldt, J. Torsti, AGU Monograph Series (AGU, Washington, 2006), p. 283
E.A. Lucek, T.S. Horbury, I. Dandouras, H. Reme, Cluster observations of the Earth's quasi-parallel bow shock. J. Geophys. Res. **113**, A07S02 (2008). doi:10.1029/2007JA012756

G. Mann, A. Klassen, H. Aurass, H.-T. Classen, Formation and development of shock waves in the solar corona and the near-Sun interplanetary space. Astron. Astrophys. **400**, 329 (2003)
G.M. Mason et al., Particle acceleration and sources in the November 1997 solar energetic particle events. Geophys. Res. Lett. **26**, 141 (1999a)
G.M. Mason, J.E. Mazur, J.R. Dwyer, ^{3}He enhancements in large solar energetic particle events. Astrophys. J. **525**, L133 (1999b)
G.M. Mason et al., Abundances of heavy and ultraheavy ions in ^{3}He-rich solar flares. Astrophys. J. **606**, 555 (2004)
S. Masson et al., Acceleration of relativistic protons during the 20 January 2005 flare and CME. Sol. Phys. **257**, 305 (2009)
J.E. Mazur, G.M. Mason, M.D. Looper, R.A. Leske, R.A. Mewaldt, Charge states of solar energetic particles using the geomagnetic cutoff technique: SAMPEX measurements in the 6 November 1997 solar particle event. Geophys. Res. Lett. **26**, 173 (1999)
D.J. McComas, N.A. Schwadron, An explanation of the Voyager paradox: particle acceleration at a blunt termination shock. Geophys. Res. Lett. **33**, L04102 (2006). doi:10.1029/2005GL025437
K.G. McCracken, H. Moraal, P.H. Stoker, Investigation of the multiple-component structure of the 20 January 2005 cosmic ray ground level enhancement. J. Geophys. Res. **113**, A12101 (2008). doi:10.1029/2007JA012829
R.B. McKibben, Azimuthal propogation of low-energy solar-flare protons as observed from spacecraft very widely separated in solar azimuth. J. Geophys. Res. **77**, 3957 (1972)
R.A. Mewaldt, Solar energetic particle composition, energy spectra, and space weather. Space Sci. Rev. **124**, 303 (2007). doi:10.1007/s11214-006-9091-0
R.A. Mewaldt et al. (eds.), *Acceleration and Transport of Energetic Particles Observed in the Heliosphere: ACE 2000 Symposium*. AIP Conference Proceedings, vol. 528 (2000). Cover picture
R.A. Mewaldt et al., Proton, helium, and electron spectra during the large solar particle events of October-November 2003. J. Geophys. Res. **110**, A09S18 (2005). doi:10.1029/2005JA011038
R.A. Mewaldt, C.M.S. Cohen, G.M. Mason, The source material for large solar energetic particle events, in *Solar Eruptions and Energetic Particles*, ed. by N. Gopalswamy, R.A. Mewaldt, J. Torsti, AGU Monograph Series, vol. 165 (2006), p. 115
R.A. Mewaldt et al., On the differences in composition between solar energetic particles and solar wind. Space Sci. Rev. **130**, 207 (2007)
R.A. Mewaldt et al., How efficient are coronal mass ejections at accelerating solar energetic particles? in *Particle Acceleration and Transport in the Heliosphere and Beyond*. AIP Conference Proceedings, vol. 1039 (2008), p. 111
R.A. Mewaldt et al., STEREO observations of energetic neutral hydrogen atoms during the 2006 December 5 solar flare. Astrophys. J. **693**, L11 (2009)
R.A. Mewaldt et al., Observations and interpretations of energetic neutral hydrogen atoms from the December 5, 2006 solar event, in *Twelfth International Solar Wind Conference*. AIP Conference Proceedings, vol. 1216 (AIP, New York, 2010), p. 592
R.A. Mewaldt et al., Energy spectra, composition, and other properties of ground-level events during Solar Cycle 23. Space Sci. Rev. (2012). doi:10.1007/s11214-012-9884-2
P.M. Morse, H. Feshbach, *Methods of Theoretical Physics* (McGraw-Hill, New York, 1953), pp. 865–869
M. Neugebauer, J. Giacalone, Multispacecraft observations of interplanetary shocks: nonplanarity and energetic particles. J. Geophys. Res. **110**, A12106 (2005). doi:10.1029/2005JA011380
M. Neugebauer et al., Encounter of the Ulysses spacecraft with the ion tail of Comet McNaught. Astrophys. J. **667**, 1262 (2007)
C.K. Ng, D.V. Reames, Focused interplanetary transport of approximately 1 MeV solar energetic protons through self-generated Alfvén waves. Astrophys. J. **424**, 1032 (1994)
C.K. Ng, D.V. Reames, A.J. Tylka, Effect of proton-amplified waves on the evolution of solar energetic particle composition in gradual events. Geophys. Res. Lett. **26**, 2145 (1999)
V. Ontiveros, A. Vourlidas, Quantitative measurements of coronal mass ejection-driven shocks from LASCO observations. Astrophys. J. **693**, 267 (2009)
E.N. Parker, The passage of energetic charged particles through interplanetary space. Planet. Space Sci. **13**, 9 (1965)
G. Paschmann et al., Characteristics of reflected and diffuse ions upstream from the Earth's bow shock. J. Geophys. Res. **86**, 4355 (1981)
V.S. Ptuskin, Cosmic-ray acceleration by long-wave turbulence. Pis'ma Astron. Zh. **14**, 599 (1988)
V.S. Ptuskin, Propagation, confinement models, and large-scale dynamical effects of galactic cosmic rays. Space Sci. Rev. **99**, 281 (2001)
K.R. Pyle, J.A. Simpson, A. Barnes, J.D. Mihalov, Shock acceleration of nuclei and electrons in the heliosphere beyond 24 AU. Astrophys. J. **282**, 107 (1984)

J.C. Raymond, S. Krucker, R.P. Lin, V. Petrosian, Observational aspects of particle acceleration in large solar flares. Space Sci. Rev. (2012, this issue). doi:10.1007/s11214-012-9897-x
D.V. Reames, Acceleration of energetic particles by shock waves from large solar flares. Astrophys. J. **358**, L63 (1990)
D.V. Reames, Coronal abundances determined from energetic particles. Adv. Space Res. **15**, 41 (1995)
D.V. Reames, Particle acceleration by CME-driven shock waves, in *Proc. Int. Conf. Cosmic Rays 26th*. AIP Conference Proceedings, vol. 516 (AIP, New York, 2000), pp. 289–300
D.V. Reames, C.K. Ng, Streaming-limited intensities of solar energetic particles. Astrophys. J. **504**, 1002 (1998)
D.V. Reames, C.K. Ng, Streaming-limited intensities of solar energetic particles on the intensity plateau. Astrophys. J. **723**, 1286 (2010)
D.V. Reames et al., Energy spectra of ions accelerated in impulsive and gradual solar events. Astrophys. J. **483**, 515 (1997a)
D.V. Reames, S.W. Kahler, C.K. Ng, Spatial and temporal invariance in the spectra of energetic particles in gradual solar events. Astrophys. J. **491**, 414 (1997b)
D.V. Reames et al., Late-phase acceleration of energetic ions in corotating interaction regions. Geophys. Res. Lett. **24**, 2917 (1997c)
E.C. Roelof, Propagation of solar cosmic rays in the interplanetary magnetic field, in *Lectures in High-Energy Astrophysics*, ed. by H. Ögelman, J.R. Wayland, NASA SP-199 (NASA, Washington, 1969), p. 111
E.T. Sarris, J.A. Van Allen, Effects of interplanetary shock waves on energetic charged particles. J. Geophys. Res. **79**, 4157 (1974)
K.M. Schure, A.R. Bell, L. O'C. Drury, A.M. Bykov, Diffusive shock acceleration and magnetic field amplification. Space Sci. Rev. (2012, this issue). doi:10.1007/s11214-012-9871-7
N.A. Schwadron, D.J. McComas, Pickup ions from energetic neutral atoms. Astrophys. J. **712**, L157 (2010)
N.A. Schwadron, M.A. Lee, D.J. McComas, Diffusive acceleration at the blunt termination shock. Astrophys. J. **675**, 1584 (2008)
S.J. Schwartz, D. Burgess, Quasi-parallel shocks—a patchwork of three-dimensional structures. Geophys. Res. Lett. **18**, 373 (1991)
E.C. Stone et al., The advanced composition explorer. Space Sci. Rev. **86**, 1 (1998)
B.T. Tsurutani, E.J. Smith, D.E. Jones, Waves observed upstream of interplanetary shocks. J. Geophys. Res. **88**, 5645 (1983)
A.J. Tylka, W.F. Dietrich, A new and comprehensive analysis of proton spectra in ground-level enhanced (GLE) solar particle events, in *Int. Cosmic Ray Conf. 31st* (2009). http://icrc2009.uni.lodz.pl/proc/pdf/icrc0273.pdf
A.J. Tylka, M.A. Lee, A model for spectral and compositional variability at high energies in large, gradual solar particle events. Astrophys. J. **646**, 1319 (2006)
A.J. Tylka, D.V. Reames, C.K. Ng, Observations of systematic temporal evolution in elemental composition during gradual solar energetic particle events. Geophys. Res. Lett. **26**, 2141 (1999)
A.J. Tylka, P.R. Boberg, R.E. McGuire, C.K. Ng, D.V. Reames, Temporal evolution in the spectra of gradual solar energetic particle events, in *Acceleration and Transport of Energetic Particles Observed in the Heliosphere: ACE 2000 Symposium*, ed. by R.A. Mewaldt et al., AIP Conference Proceedings, vol. 528 (AIP, New York, 2000), pp. 147–152
A.J. Tylka et al., Evidence for remnant flare suprathermals in the source population of solar energetic particles in the 2000 Bastille Day event. Astrophys. J. **558**, L59 (2001)
A.J. Tylka et al., Shock geometry, seed populations, and the origin of variable elemental composition at high energies in large gradual solar particle events. Astrophys. J. **625**, 474 (2005)
R. Vainio, On the generation of Alfvén waves by solar energetic particles. Astron. Astrophys. **406**, 735 (2003)
P. van Nes, R. Reinhard, T.R. Sanderson, K.-P. Wenzel, R.D. Zwickl, The energy spectrum of 35- to 1600-keV protons associated with interplanetary shocks. J. Geophys. Res. **89**, 2122 (1984)
L. Wang, R.P. Lin, S. Krucker, G.M. Mason, A statistical study of solar electron events over one solar cycle. Astrophys. J. (2012, submitted)
M.E. Wiedenbeck et al., How common is energetic ^{3}He in the inner heliosphere? in *Solar Wind 10 Proceedings of the Tenth International Solar Wind Conference*, ed. by M. Velli, R. Bruno, F. Malara, AIP Conf. Proc., vol. 679 (AIP, New York, 2003), pp. 652–655
G.P. Zank, G. Li, V. Florinski, Q. Hu, D. Lario, C.W. Smith, Particle acceleration at perpendicular shock waves: model and observations. J. Geophys. Res. **111**, A06108 (2006). doi:10.1029/2005JA011524
M. Zhang, M.A. Lee, Stochastic acceleration of energetic particles in the heliosphere. Space Sci. Rev. (2011). doi:10.1007/s11214-011-9754-3